



Phase shifts of the light pseudoscalar meson and heavy meson scattering in heavy meson chiral perturbation theory

Bo-Lin Huang^a , Zi-Yang Lin, Kan Chen, Shi-Lin Zhu^b

School of Physics and Center of High Energy Physics, Peking University, Beijing 100871, China

Received: 23 June 2022 / Accepted: 17 January 2023 / Published online: 25 January 2023
© The Author(s) 2023

Abstract We calculate the complete T matrices of the elastic light pseudoscalar meson and heavy meson scattering to the third order in heavy meson chiral perturbation theory. We determine the low-energy constants by fitting the phase shifts and scattering lengths from lattice QCD simulations simultaneously and predict the phase shifts at the physical meson masses. The phase shifts in the $D\pi$ ($I = 1/2$), DK ($I = 0$), $D\bar{K}$ ($I = 0$), $D_s\bar{K}$, $D\eta$ and $D_s\eta$ S waves are so strong that bound states or resonances may be generated dynamically in all these channels. The DK ($I = 0$) channel corresponds to the well-known exotic state $D_{s0}^*(2317)$. The DK ($I = 0$) channel corresponds to the well-known exotic state $D_{s0}^*(2317)$. The coupled-channel $D\pi$, $D\eta$ and $D_s\bar{K}$ scattering corresponds to $D_0^*(2400)$. The coupled-channel $D\pi$, $D\eta$ and $D_s\bar{K}$ scattering corresponds to $D_0^*(2400)$. We also predict the scattering lengths and scattering volumes and observe good convergence in the scattering volumes. Our calculations provide a possibility to accurately investigate the exotic state in the light pseudoscalar meson and heavy meson interactions.

1 Introduction

Investigations of the meson–meson scattering allow to discover interesting features of quantum chromodynamics (QCD) at hadronic energy scales, and also provide a basis for further research on hadron spectroscopy. In the past decades, the precision experimental data involving the charm quark have revealed many surprising features in hadron spectroscopy. For instance, some of the charmonium-like XYZ states lie very close to the two-meson thresholds.

As the fundamental theory of strong interaction, QCD becomes nonperturbative at low energies. Therefore, it is very

difficult to use perturbative methods to derive the meson–meson interactions. Weinberg proposed an effective field theory (EFT) for the purpose of solving this problem in a seminal paper [1]. The EFT is formulated in terms of the most general Lagrangian consistent with the general symmetry principles, and the degrees of freedom are hadrons at low energy. The corresponding formalism is called chiral perturbation theory (ChPT) [2]. ChPT is a useful and efficient tool to study hadronic physics at low energies [3]. However, a power-counting problem in heavy hadron ChPT occurs because of the nonvanishing heavy hadron mass in the chiral limit. Heavy baryon chiral perturbation theory (HBChPT) was proposed and developed to solve the power-counting problem that occurs in baryon ChPT [4–6]. Many achievements have been obtained in the light flavor hadronic physics using SU(2) HBChPT [7–14]. Furthermore, the investigations in the SU(3) HBChPT also led to reasonable predictions [15–22]. The infrared regularization of the covariant baryon ChPT [23] and the extended-on-mass-shell scheme [24, 25] for solving the power-counting problem are two popular relativistic approaches and have led to substantial progress in many aspects as documented in Refs. [26–32].

However, HBChPT is still a well-established and versatile tool for the study of the low-energy hadronic physics. The expansion in HBChPT is expanded simultaneously in terms of p/Λ_χ and p/M_0 , where p represents the meson momentum or its mass or the small residue momentum of a baryon in the nonrelativistic limit. Similar to the HBChPT formalism in the light flavor meson–baryon and baryon–baryon interactions, we can use the heavy meson chiral perturbation theory (HMChPT) to address the charmed mesons, as done in Ref. [33]. This framework can also be extended to the heavy flavor hadron interactions and new hadron states [34–37] (for a review of the heavy hadron systems in ChPT, see Refs. [38]).

^a e-mail: blhuang@pku.edu.cn (corresponding author)

^b e-mail: zhysl@pku.edu.cn

Since the discoveries of the charm-strange meson $D_{s0}^*(2317)$ [39–41] and the hidden-charm meson $X(3872)$ [42], many investigations have been devoted to various exotic states that cannot be classified into conventional hadrons [43–55]. The $D_{s0}^*(2317)$ has inspired various explanations with the different methods and pictures [56–69] (for a detailed review see Ref. [70]). Some lattice QCD simulations [65, 66, 68] seem to support the interpretation of the $D_{s0}^*(2317)$ as a DK molecule. Thus, a detailed study of the DK scattering will help us to understand the nature of this exotic state. However, in lattice calculations, the light pseudoscalar meson masses are always larger than their physical masses because of the shortage of computational resources at physical quark masses. Therefore, the extrapolation of the light pseudoscalar meson and heavy meson scattering from the nonphysical meson mass to the physical value is necessary with the help of ChPT.

In our previous papers [71, 72], we calculated the light pseudoscalar meson and heavy meson scattering lengths up to $\mathcal{O}(p^4)$ in HMChPT. The scattering lengths were calculated through both perturbative and iterated methods as described in Ref. [72]. The value of the scattering length for the channel $DK(I=0)$, which involves $D_{s0}^*(2317)$, was obtained correctly with the iterated method. In fact, the channel $DK(I=0)$ has a sufficiently strong attractive interaction and can lead to a quasi-bound state with the iterated methods, as shown in Refs. [65, 73–79]. Note that a repulsive interaction has a negative scattering length or phase shift in our convention. The scattering length is an important quantity of the scattering process, which encodes the information of the underlying interaction.

The partial-wave phase shifts contain the complete information of a scattering process in the physical region. In this work, our study is concerned not only with the scattering lengths but also with the partial-wave phase shifts. We calculate the complete T matrices of the elastic pseudoscalar meson and heavy meson scattering to the third order in HMChPT. Then, we determine the low-energy constants (LECs) by fitting the phase shifts and scattering lengths simultaneously. From the complete pseudoscalar meson and heavy meson scattering amplitudes up to $\mathcal{O}(p^3)$, we can judge directly whether the attraction in a scattering channel is strong enough to generate a bound state. Furthermore, the detailed features of QCD at hadronic energy scales can be obtained from the phase shifts based on the $\mathcal{O}(p^3)$ calculation. Hopefully, the phase shifts of the light meson and heavy meson scattering (e.g., the D^-K^+ channel) may be extracted from the LHCb group or BelleII measurements in the future.

This paper is organized as follows. In Sect. 2, the chiral Lagrangians are presented up to $\mathcal{O}(p^3)$. In Sect. 3, the Feynman diagrams and the results of the T matrices are presented. In Sect. 4, we outline how to derive partial-wave phase shifts

and scattering lengths from the T matrices. Section 5 contains the numerical results and discussions. The last section gives a brief summary.

2 Chiral Lagrangian

Our calculation of the elastic light pseudoscalar meson and heavy meson scattering is based on the effective chiral Lagrangian in HMChPT,

$$\mathcal{L}_{\text{eff}} = \mathcal{L}_{\phi\phi} + \mathcal{L}_{H\phi}. \quad (1)$$

Here, the SU(3) matrix ϕ represents the pseudoscalar Goldstone fields ($\phi = \pi, K, \bar{K}, \eta$). The lowest-order chiral Lagrangian for the Goldstone meson–meson interaction takes the form [80]

$$\mathcal{L}_{\phi\phi}^{(2)} = f^2 \text{tr} \left(u_\mu u^\mu + \frac{\chi_+}{4} \right). \quad (2)$$

The axial vector quantity $u^\mu = \frac{i}{2} \{ \xi^\dagger, \partial^\mu \xi \}$ contains an odd number of meson fields. The SU(3) matrix $U = \xi^2 = \exp(i\phi/f)$ collects the pseudoscalar Goldstone boson fields. The quantities $\chi_\pm = \xi^\dagger \chi \xi^\dagger \pm \xi \chi \xi$ with $\chi = \text{diag}(m_\pi^2, m_\pi^2, 2m_K^2 - m_\pi^2)$ introduce explicit chiral symmetry breaking terms. The parameter f is the pseudoscalar decay constant in the chiral limit. The lowest-order chiral Lagrangian for the heavy mesons in the heavy quark symmetry limit can be written as

$$\mathcal{L}_{H\phi}^{(1)} = - \langle (i v \cdot \partial H) \bar{H} \rangle + \langle H v \cdot \Gamma \bar{H} \rangle + g \langle H u_\mu \gamma^\mu \gamma_5 \bar{H} \rangle, \quad (3)$$

where $v_\mu = (1, 0, 0, 0)$ is the heavy meson velocity, $\langle \dots \rangle$ means the trace for gamma matrices, the chiral connection $\Gamma^\mu = \frac{i}{2} [\xi^\dagger, \partial^\mu \xi]$ contains an even number of meson fields and the doublet of the ground state heavy mesons reads

$$H = \frac{1 + \not{v}}{2} (P_\mu^* \gamma^\mu + i P \gamma_5), \\ \bar{H} = \gamma^0 H^\dagger \gamma^0 = (P_\mu^{*\dagger} \gamma^\mu + i P^\dagger \gamma_5) \frac{1 + \not{v}}{2}, \quad (4)$$

$$P = (D^0, D^+, D_s^+), \quad P_\mu^* = (D^{0*}, D^{+*}, D_s^{+*})_\mu. \quad (5)$$

For the calculation of the complete T matrices up to the third order, the heavy meson Lagrangians $\mathcal{L}_{H\phi}^{(2)}$ and $\mathcal{L}_{H\phi}^{(3)}$ in the heavy quark symmetry limit read

$$\mathcal{L}_{H\phi}^{(2)} = c_0 \langle H \bar{H} \rangle \text{tr}(\chi_+) + c_1 \langle H \chi_+ \bar{H} \rangle \\ - c_2 \langle H \bar{H} \rangle \text{tr}(v \cdot u v \cdot u) - c_3 \langle H v \cdot u v \cdot u \bar{H} \rangle$$

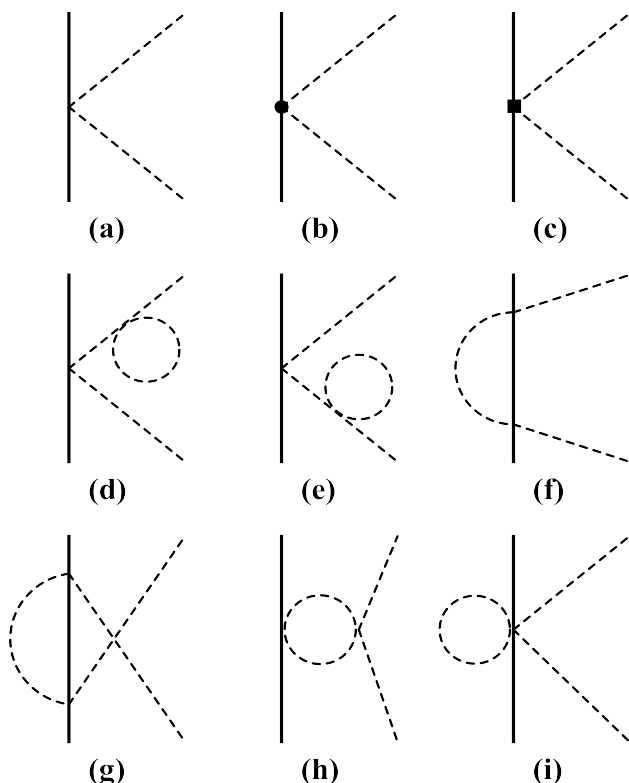


Fig. 1 Tree and nonvanishing loop diagrams in the calculation of the Goldstone-heavy meson scattering amplitudes to the third order in HMChPT. The dashed lines represent the Goldstone bosons and solid lines represent the pseudoscalar heavy mesons. The heavy dots and filled squares refer to the vertices from $\mathcal{L}_{H\phi}^{(2)}$ and $\mathcal{L}_{H\phi}^{(3)}$, respectively

$$-c_4 \langle H \bar{H} \rangle \text{tr}(u^\mu u_\mu) - c_5 \langle H u^\mu u_\mu \bar{H} \rangle, \tag{6}$$

$$\begin{aligned} \mathcal{L}_{H\phi}^{(3)} = & \kappa_1 \langle H[\chi_-, v \cdot u] \bar{H} \rangle \\ & + i\kappa_2 \langle H[v \cdot u, [v \cdot \partial, v \cdot u]] \bar{H} \rangle \\ & + i\kappa_3 \langle H[u^\mu, [v \cdot \partial, u_\mu]] \bar{H} \rangle. \end{aligned} \tag{7}$$

3 T matrices

In this work, we are considering only the elastic light pseudoscalar meson and heavy meson scattering processes $M(\mathbf{q}) + H(-\mathbf{q}) \rightarrow M(\mathbf{q}') + H(-\mathbf{q}')$ in the center-of-mass frame with $|\mathbf{q}| = |\mathbf{q}'| = q$. The leading order (LO) amplitudes resulting from diagram (a) in Fig. 1 read

$$\begin{aligned} T_{\pi D}^{(1/2, \text{LO})} &= \frac{2w_\pi}{f_\pi^2}, & T_{\pi D}^{(3/2, \text{LO})} &= -\frac{w_\pi}{f_\pi^2}, \\ T_{\pi D_s}^{(\text{LO})} &= 0, & T_{KD}^{(1, \text{LO})} &= 0, & T_{KD}^{(0, \text{LO})} &= \frac{2w_K}{f_K^2}, \\ T_{KD_s}^{(\text{LO})} &= -\frac{w_K}{f_K^2}, & T_{\bar{K}D}^{(1, \text{LO})} &= -\frac{w_K}{f_K^2}, \end{aligned}$$

$$T_{\bar{K}D}^{(0, \text{LO})} = \frac{w_K}{f_K^2}, \quad T_{\bar{K}D_s}^{(\text{LO})} = \frac{w_K}{f_K^2}, \quad T_{\eta D}^{(\text{LO})} = 0, \quad T_{\eta D_s}^{(\text{LO})} = 0, \tag{8}$$

where $K = (K^+, K^0)^T$, $\bar{K} = (\bar{K}^0, K^-)^T$. The first superscripts of the T matrices denote the total isospin. In the channels with an isoscalar η -meson or D_s -meson, the total isospin is unique and does not need to be specified. The quantities $w_\phi = (m_\phi^2 + q^2)^{1/2}$ with $\phi = (\pi, K, \eta)$ denote the center-of-mass energy of the light pseudoscalar mesons. We take the renormalized decay constants f_ϕ with the nonzero quark mass instead of f in the chiral limit.

At the next-to-leading order (NLO), one has the contributions from diagram (b) of Fig. 1, which involves the vertex from the Lagrangian $\mathcal{L}_{H\phi}^{(2)}$. The amplitudes involving the low-energy constants (LECs) read

$$\begin{aligned} T_{\pi D}^{(1/2, \text{NLO})} &= \frac{1}{f_\pi^2} [8c_0 m_\pi^2 + 4c_1 m_\pi^2 + 2c_2 w_\pi^2 + c_3 w_\pi^2 \\ &+ 2c_4 (w_\pi^2 - q^2 z) + c_5 (w_\pi^2 - q^2 z)], \end{aligned} \tag{9}$$

$$\begin{aligned} T_{\pi D}^{(3/2, \text{NLO})} &= \frac{1}{f_\pi^2} [8c_0 m_\pi^2 + 4c_1 m_\pi^2 + 2c_2 w_\pi^2 + c_3 w_\pi^2 \\ &+ 2c_4 (w_\pi^2 - q^2 z) + c_5 (w_\pi^2 - q^2 z)], \end{aligned} \tag{10}$$

$$T_{\pi D_s}^{(\text{NLO})} = \frac{1}{f_\pi^2} [8c_0 m_\pi^2 + 2c_2 w_\pi^2 + 2c_4 (w_\pi^2 - q^2 z)], \tag{11}$$

$$T_{KD}^{(1, \text{NLO})} = \frac{1}{f_K^2} [8c_0 m_K^2 + 2c_2 w_K^2 + 2c_4 (w_K^2 - q^2 z)], \tag{12}$$

$$\begin{aligned} T_{KD}^{(0, \text{NLO})} &= \frac{1}{f_K^2} [8c_0 m_K^2 + 8c_1 m_K^2 + 2c_2 w_K^2 + 2c_3 w_K^2 \\ &+ 2c_4 (w_K^2 - q^2 z) + 2c_5 (w_K^2 - q^2 z)], \end{aligned} \tag{13}$$

$$\begin{aligned} T_{KD_s}^{(\text{NLO})} &= \frac{1}{f_K^2} [8c_0 m_K^2 + 4c_1 m_K^2 + 2c_2 w_K^2 + c_3 w_K^2 \\ &+ 2c_4 (w_K^2 - q^2 z) + c_5 (w_K^2 - q^2 z)], \end{aligned} \tag{14}$$

$$\begin{aligned} T_{\bar{K}D}^{(1, \text{NLO})} &= \frac{1}{f_K^2} [8c_0 m_K^2 + 4c_1 m_K^2 + 2c_2 w_K^2 + c_3 w_K^2 \\ &+ 2c_4 (w_K^2 - q^2 z) + c_5 (w_K^2 - q^2 z)], \end{aligned} \tag{15}$$

$$\begin{aligned} T_{\bar{K}D}^{(0, \text{NLO})} &= \frac{1}{f_K^2} [8c_0 m_K^2 - 4c_1 m_K^2 + 2c_2 w_K^2 - c_3 w_K^2 \\ &+ 2c_4 (w_K^2 - q^2 z) - c_5 (w_K^2 - q^2 z)], \end{aligned} \tag{16}$$

$$\begin{aligned} T_{\bar{K}D_s}^{(\text{NLO})} &= \frac{1}{f_K^2} [8c_0 m_K^2 + 4c_1 m_K^2 + 2c_2 w_K^2 + c_3 w_K^2 \\ &+ 2c_4 (w_K^2 - q^2 z) + c_5 (w_K^2 - q^2 z)], \end{aligned} \tag{17}$$

$$\begin{aligned} T_{\eta D}^{(\text{NLO})} &= \frac{1}{3f_\eta^2} [24c_0 m_\eta^2 + 4c_1 m_\pi^2 + 6c_2 w_\eta^2 + c_3 w_\eta^2 \\ &+ 6c_4 (w_\eta^2 - q^2 z) + c_5 (w_\eta^2 - q^2 z)], \end{aligned} \tag{18}$$

$$T_{\eta D_s}^{(NLO)} = \frac{1}{3f_\eta^2} [24c_0 m_\eta^2 + 16c_1 (2m_K^2 - m_\pi^2) + 6c_2 w_\eta^2 + 4c_3 w_\eta^2 + 6c_4 (w_\eta^2 - q^2 z) + 4c_5 (w_\eta^2 - q^2 z)], \tag{19}$$

where $z = \cos \theta$ is the cosine of the angle θ between \mathbf{q} and \mathbf{q}' .

At the next-to-next-to-leading order (N2LO), one has contributions from diagram (c) in Fig. 1, which involves the vertex from the Lagrangian $\mathcal{L}_{H\phi}^{(3)}$. The amplitudes read

$$T_{\pi D}^{(1/2, N2LO)} = \frac{1}{f_\pi^2} [16\bar{k}_1 m_\pi^2 w_\pi + 4\bar{k}_2 w_\pi^3 + 4\bar{k}_3 w_\pi (w_\pi^2 - q^2 z)], \tag{20}$$

$$T_{\pi D}^{(3/2, N2LO)} = \frac{1}{f_\pi^2} [-8\bar{k}_1 m_\pi^2 w_\pi - 2\bar{k}_2 w_\pi^3 - 2\bar{k}_3 w_\pi (w_\pi^2 - q^2 z)], \tag{21}$$

$$T_{\pi D_s}^{(N2LO)} = 0, \tag{22}$$

$$T_{K D}^{(1, N2LO)} = 0, \tag{23}$$

$$T_{K D}^{(0, N2LO)} = \frac{1}{f_K^2} [16\bar{k}_1 m_K^2 w_K + 4\bar{k}_2 w_K^3 + 4\bar{k}_3 w_K (w_K^2 - q^2 z)], \tag{24}$$

$$T_{K D_s}^{(N2LO)} = \frac{1}{f_K^2} [-8\bar{k}_1 m_K^2 w_K - 2\bar{k}_2 w_K^3 - 2\bar{k}_3 w_K (w_K^2 - q^2 z)], \tag{25}$$

$$T_{\bar{K} D}^{(1, N2LO)} = \frac{1}{f_{\bar{K}}^2} [-8\bar{k}_1 m_{\bar{K}}^2 w_K - 2\bar{k}_2 w_K^3 - 2\bar{k}_3 w_K (w_K^2 - q^2 z)], \tag{26}$$

$$T_{\bar{K} D}^{(0, N2LO)} = \frac{1}{f_{\bar{K}}^2} [8\bar{k}_1 m_{\bar{K}}^2 w_K + 2\bar{k}_2 w_K^3 + 2\bar{k}_3 w_K (w_K^2 - q^2 z)], \tag{27}$$

$$T_{\bar{K} D_s}^{(N2LO)} = \frac{1}{f_{\bar{K}}^2} [8\bar{k}_1 m_{\bar{K}}^2 w_K + 2\bar{k}_2 w_K^3 + 2\bar{k}_3 w_K (w_K^2 - q^2 z)], \tag{28}$$

$$T_{\eta D}^{(N2LO)} = 0, \tag{29}$$

$$T_{\eta D_s}^{(N2LO)} = 0. \tag{30}$$

At this order, one also has the amplitudes from the one-loop diagrams. The nonvanishing one-loop diagrams generated by the vertices of $\mathcal{L}_{\phi\phi}^{(2)}$ and $\mathcal{L}_{H\phi}^{(1)}$ are shown in the second and third row of Fig. 1. Note that the third-order scale-independent LECs \bar{k}_1 , \bar{k}_2 and \bar{k}_3 are used in the counterterm T matrices, as done in Ref. [9]. Putting all amplitudes from the different one-loop diagrams together, we have

$$T_{\pi D}^{(1/2, LOOP)} = -\frac{w_\pi}{12f_\pi^4} \{3w_\pi [3J_0(-w_\pi, m_K) + 4J_0(-w_\pi, m_\pi) - 9J_0(w_\pi, m_K) - 17J_0(w_\pi, m_\pi)] + 12I_2(t, m_K) + 16I_2(t, m_\pi)\}, \tag{31}$$

$$T_{\pi D}^{(3/2, LOOP)} = \frac{w_\pi}{6f_\pi^4} \{3w_\pi [3J_0(-w_\pi, m_K) + 7J_0(-w_\pi, m_\pi)$$

$$+ J_0(w_\pi, m_\pi)] + 3I_2(t, m_K) + 4I_2(t, m_\pi)\}, \tag{32}$$

$$T_{\pi D_s}^{(LOOP)} = \frac{w_\pi^2}{2f_\pi^4} [J_0(w_\pi, m_K) + J_0(-w_\pi, m_K)], \tag{33}$$

$$T_{K D}^{(1, LOOP)} = \frac{w_K}{2f_K^4} \{w_K [J_0(-w_K, m_K) + J_0(w_K, m_\pi)] + 2I_2(t, m_\pi) - I_2(t, m_K)\}, \tag{34}$$

$$T_{K D}^{(0, LOOP)} = \frac{w_K}{12f_K^4} \{3w_K [2J_0(-w_K, m_K) + 24J_0(w_K, m_\eta) + 22J_0(w_K, m_K) + J_0(w_K, m_\pi)] - 10I_2(t, m_K) - 36I_2(t, m_\pi)\}, \tag{35}$$

$$T_{K D_s}^{(LOOP)} = \frac{w_K}{12f_K^4} \{3w_K [12J_0(-w_K, m_\eta) + 7J_0(-w_K, m_K) + 5J_0(-w_K, m_\pi) + 2J_0(w_K, m_K)] + 14I_2(t, m_K)\}, \tag{36}$$

$$T_{\bar{K} D}^{(1, LOOP)} = \frac{w_K}{24f_K^4} \{3w_K [24J_0(-w_K, m_\eta) + 22J_0(-w_K, m_K) + 3J_0(-w_K, m_\pi) + 4J_0(w_K, m_K)] + 16I_2(t, m_K) + 24I_2(t, m_\pi)\}, \tag{37}$$

$$T_{\bar{K} D}^{(0, LOOP)} = \frac{w_K}{24f_K^4} \{3w_K [-24J_0(-w_K, m_\eta) - 22J_0(-w_K, m_K) + 5J_0(-w_K, m_\pi) + 4J_0(w_K, m_K)] + 8I_2(t, m_K) - 72I_2(t, m_\pi)\}, \tag{38}$$

$$T_{\bar{K} D_s}^{(LOOP)} = \frac{w_K}{12f_K^4} \{3w_K [2J_0(-w_K, m_K) + 12J_0(w_K, m_\eta) + 7J_0(w_K, m_K) + 5J_0(w_K, m_\pi)] - 14I_2(t, m_K)\}, \tag{39}$$

$$T_{\eta D}^{(LOOP)} = \frac{3w_\eta^2}{4f_\eta^4} [J_0(-w_\eta, m_K) + J_0(w_\eta, m_K)], \tag{40}$$

$$T_{\eta D_s}^{(LOOP)} = \frac{21w_\eta^2}{8f_\eta^4} [J_0(-w_\eta, m_K) + J_0(w_\eta, m_K)], \tag{41}$$

with the finite parts of loop functions

$$J_0(w, m) = \frac{w}{8\pi^2} + \begin{cases} \frac{1}{4\pi^2} \sqrt{w^2 - m^2} \ln \frac{-w + \sqrt{w^2 - m^2}}{m} & (w < -m), \\ -\frac{1}{4\pi^2} \sqrt{m^2 - w^2} \arccos \frac{-w}{m} & (-m < w < m), \\ \frac{1}{4\pi^2} \sqrt{w^2 - m^2} \left(i\pi - \ln \frac{w + \sqrt{w^2 - m^2}}{m} \right) & (w > m), \end{cases} \tag{42}$$

$$I_2(t, m) = \frac{1}{48\pi^2} \left\{ 2m^2 - \frac{5t}{12} - \frac{(4m^2 - t)^{3/2}}{2\sqrt{-t}} \ln \frac{\sqrt{4m^2 - t} + \sqrt{-t}}{2m} \right\}, \tag{43}$$

and the squared invariant momentum transfer $t = 2q^2(z - 1)$.

4 Partial-wave phase shifts and scattering lengths

The partial-wave amplitudes $f_l^{(I)}(q)$, where l refers to the orbital angular momentum, are obtained from the T matrix

by a projection:

$$f_l^{(I)}(q) = \frac{M_H}{16\pi\sqrt{s}} \int_{-1}^{+1} dz [T_{\phi H}^{(I)} P_l(z)], \tag{44}$$

where $P_l(z)$ denotes the conventional Legendre polynomial and $\sqrt{s} = (m_\phi^2 + q^2)^{1/2} + (M_H^2 + q^2)^{1/2}$ is the total center-of-mass energy. For the channels that may generate the bound states or resonances, the T matrix must be iterated to the infinite order. We consider the T matrix up to the third order only in the calculation of the phase shifts and scattering lengths since we do not aim to achieve the description of the bound states or resonances. For the energy range considered in this paper, the phase shifts without the effect of the bound states or resonances $\delta_l^{(I)}(q)$ are calculated by (also see Refs. [9, 81])

$$\delta_l^{(I)}(q) = \arctan[q \operatorname{Re} f_l^{(I)}(q)]. \tag{45}$$

Based on relativistic kinematics, there is a relation between the center-of-mass momentum and the momentum of the incident light pseudoscalar meson in the laboratory system,

$$q^2 = \frac{M_H^2 p_{\text{lab}}^2}{m_\phi^2 + M_H^2 + 2M_H \sqrt{m_\phi^2 + p_{\text{lab}}^2}}. \tag{46}$$

The scattering lengths for the S waves and the scattering volumes for P waves are obtained by dividing out the threshold behavior of the respective partial-wave amplitude and approaching the threshold [82]

$$a_l^{(I)} = \lim_{q \rightarrow 0} q^{-2l} f_l^{(I)}(q). \tag{47}$$

5 Results and discussion

In order to determine the low-energy constants, we start by fitting both phase shifts and scattering lengths from lattice QCD simulations at the nonphysical meson values simultaneously, and we then make predictions for the phase shifts and the threshold parameters in all channels at the physical meson values.

5.1 Fitting

Now, we determine $c_{0,\dots,5}$ and $\bar{\kappa}_{1,2,3}$ using the phase shifts and the scattering lengths from lattice data. We take the S -wave phase shifts with $I = 3/2$ and the P -wave phase shifts with $I = 1/2$ of the elastic $D\pi$ scattering at $m_\pi \simeq 391$ MeV from Ref. [83]. The S -wave phase shift with $I = 1/2$ of the $D\pi$ scattering is not used in the fitting because there exists a near-threshold bound state that cannot be obtained in the perturbative method. The P -wave phase shift with $I = 0$ of

the elastic DK scattering at $m_\pi \simeq 239$ MeV is taken from Ref. [68]. Again, there exists a bound state, i.e., $D_{s0}^*(2317)$, in the S -wave $I = 0$ DK channel, and then the phase shift from this channel is not used to determine the LECs. The phase shifts of the elastic $D\bar{K}$ scattering are obtained by using a simple parametrization with the scattering lengths in Ref. [68]. Therefore, we use the $D\bar{K}$ scattering lengths directly instead of the phase shifts. For the three phase shifts that are used to determine the LECs, we take the data with the pion (kaon) laboratory momentum between 5 and 300 MeV. In addition, the scattering lengths of the five channels [$D\bar{K}(I = 0)$, $D\bar{K}(I = 1)$, $D\pi(I = 3/2)$, $D_s K$, $D_s \pi$] are used to determine the LECs from Refs. [65, 68, 83]. We take the scattering length of the channel [$D\pi(I = 3/2)$] at $m_\pi \simeq 391$ MeV from Ref. [83], the scattering lengths of the channels [$D\bar{K}(I = 0)$, $D\bar{K}(I = 1)$] at $m_\pi = 239$ MeV and $m_\pi = 391$ MeV from Ref. [68], and the (M007, M010) data for the five channels from Ref. [65]. The corresponding lattice values of f_π and f_K are from Ref. [84], and we always choose $f_\eta = 1.2 f_\pi$ in this paper. The resulting LECs with the correlations between the parameters can be found in Table 1. The uncertainty for the respective parameter is statistical, and it measures how much a particular parameter can be changed while maintaining a good description of the fitting data. Nevertheless, the parameters cannot truly vary independently of each other because of the mutual correlations, as detailed in Refs. [85, 86]. Therefore, the large uncertainties of some LECs in our fit cannot make the errors of the phase shifts and the threshold parameters large because a full error analysis requires a complete covariance matrix. However, we obtain small uncertainties for some LECs (e.g., c_4 , c_5 , $\bar{\kappa}_1$). Furthermore, the values of the LECs are mostly of natural size; i.e., they are numbers of order one and the same order of magnitude as the axial vector coupling constant $g_A = 1.27$ [87, 88]. We can see that the absolute values for most of the LECs turn out to be between one and ten when one introduces dimensionless LECs (e.g., $c'_i = \Lambda_\chi c_i$). In fact, the values of the LECs in the calculations of the pion-nucleon scattering were obtained at the same order of magnitude and regarded as of natural size in Refs. [9, 10, 20, 21]. However, $c_{2,3,4}$ are around $5 - 9 \text{ GeV}^{-1}$, which may be enhanced by including $D_{s0}^*(2317)$ explicitly. In comparison, the $\Delta(1232)$ resonance enhanced the LECs in the pion-nucleon scattering. For the channel $DK(I = 0)$ involving $D_{s0}^*(2317)$, we clearly see that c_2 and c_3 can be combined into the linear combination $c_2 + c_3$, which has a small value of 0.43 GeV^{-1} . The absolute value of the correlation between c_0 and c_1 is very close to one, which is consistent with the fact that the terms with these two parameters involve only the masses of the light pseudoscalar mesons.

The corresponding phase shifts and scattering lengths from the fitting are shown in Fig. 2. The S -wave phase shifts with $I = 3/2$ and P -wave phase shifts with $I = 1/2$ of the

Table 1 Results of fitting to various lattice data of the phase shifts and scattering lengths. For a detailed description, see the main text

	Values	c_0	c_1	c_2	c_3	c_4	c_5	$\bar{\kappa}_1$	$\bar{\kappa}_2$	$\bar{\kappa}_3$
c_0 (GeV ⁻¹)	-0.77 ± 0.39	1.00	0.99	-0.86	-0.88	0.00	0.00	0.02	-0.92	0.00
c_1 (GeV ⁻¹)	-0.64 ± 0.35		1.00	-0.86	-0.89	0.00	0.00	0.01	-0.93	0.00
c_2 (GeV ⁻¹)	-5.04 ± 1.83			1.00	0.95	-0.51	-0.41	-0.01	0.61	0.50
c_3 (GeV ⁻¹)	5.47 ± 1.57				1.00	-0.36	-0.45	0.10	0.67	0.40
c_4 (GeV ⁻¹)	8.99 ± 0.93					1.00	0.80	0.00	0.37	-0.98
c_5 (GeV ⁻¹)	-3.08 ± 0.70						1.00	0.00	0.34	-0.90
$\bar{\kappa}_1$ (GeV ⁻²)	0.21 ± 0.04							1.00	0.01	0.00
$\bar{\kappa}_2$ (GeV ⁻²)	7.81 ± 3.88								1.00	-0.38
$\bar{\kappa}_3$ (GeV ⁻²)	-1.87 ± 1.47									1.00
$\chi^2/\text{d.o.f.}$	$\frac{34.85}{195-9} = 0.19$									

$D\pi$ scattering at $m_\pi \simeq 391$ MeV are in very good agreement with the data from lattice QCD simulations up to the pion laboratory momentum of 300 MeV. For the isoscalar P -wave DK scattering at $m_\pi \simeq 239$ MeV, the values of the phase shifts are very consistent with the data from lattice QCD simulations below the kaon laboratory momentum of 200 MeV. However, the P -wave phase shifts of $DK(I=0)$ from lattice QCD simulations have large errors. The values of the $DK(I=0)$ P -wave phase shifts are in agreement with the results from lattice QCD within errors up to the kaon laboratory momentum of 300 MeV. The scattering length of $D\pi(I=3/2)$ at $m_\pi \simeq 391$ MeV is in agreement with the lattice QCD value from Ref. [83] within error. The scattering lengths of $D\bar{K}(I=1)$ at $m_\pi = 239, 391$ MeV and $D\bar{K}(I=0)$ at $m_\pi = 391$ MeV are in good agreement with the values of lattice QCD from Ref. [68]. The value for $D\bar{K}(I=0)$ at $m_\pi = 239$ MeV has a small deviation from lattice QCD. The reason is that there may exist a virtual bound state in this channel. The scattering lengths of the five channels [$D\bar{K}(I=0)$, $D\bar{K}(I=1)$, $D\pi(I=3/2)$, $D_s K$, $D_s \pi$] at $m_\pi \simeq 301, 364$ MeV are in agreement with lattice QCD values from Ref. [65] within errors. There exist small deviations at a few points because the lattice QCD values are from different groups, which may cause some errors in this fitting. We have obtained a good description of the three phase shifts and the five scattering lengths at the nonphysical meson values.

Due to the strong correlations in some parameters, we use the linear combinations of the low-energy constants for further analysis. The combinations $c_2 + c_4$ and $c_3 + c_5$ contribute to the S -wave scattering. We also use $c_0 + c_1$ because they have a large correlation. Thus, we have three linear combinations instead of the separate c_i . The results can be found in Table 2. Unsurprisingly, we obtain small values and uncertainties for the three linear combinations. However, we have omitted the difference in the description of the P waves in this fitting with the linear parameter combinations. On the other

hand, the values in Table 1 can describe exactly the corresponding phase shifts and threshold parameters with the help of the mutual correlations. Therefore, it is not necessary to further analyze the phase shifts and threshold parameters in this fitting. However, we can study the reason why the values of the LECs in Table 1 are larger than the three linear combinations from Table 2. It is easy to find that the LECs in P waves are only c_4 , c_5 , and $\bar{\kappa}_3$. Thus, we fit the three LECs by using the P -wave phase shifts of the $D\pi(I=1/2)$ and $DK(I=0)$ channels. We obtain $c_4 = 13.41 \pm 0.22$ GeV⁻¹, $c_5 = -0.43 \pm 0.16$ GeV⁻¹, and $\bar{\kappa}_3 = -8.67 \pm 0.34$ GeV⁻² with a very small $\chi^2/\text{d.o.f.} = 0.01$, which is caused by the large errors in the P -wave phase shifts. Nevertheless, the large value for c_4 is also not of natural size. This may be one reason why the values in Table 1 are large. We need more precise data of the P waves to improve the LECs in Table 1.

For the channel $DK(I=0)$, we can explicitly include $D_{s0}^*(2317)$ in the fitting to improve the values of LECs. We note that the $\Lambda(1405)$ was included for the KN scattering [89] and $\Delta(1232)$ was included for the πN scattering [30]. Unfortunately, the coupling constant involving $D_{s0}^*(2317)$ has not been determined. Thus, we cannot obtain an additional constraint to determine the LECs. However, we can use the scattering length of the channel $DK(I=0)$ from lattice QCD to determine the coupling constant with $D_{s0}^*(2317)$. The value of the scattering length for the channel $DK(I=0)$ is $-1.33(20)$ fm from Ref. [64] in a near threshold lattice simulation. The corresponding formula can be found in Appendix 7. We can obtain $g_R^2 = 0.81 \pm 0.04$ by using the lattice values from Ref. [64] and the mass of the $D_{s0}^*(2317)$ from PDG [90]. The values of g_R for $D_{s0}^*(2317)$ are not very large and have the same order of magnitude as the coupling constant involving $\Lambda(1405)$ ($\bar{g}_{\Lambda R}^2 = 0.15$). Therefore, the inclusion of $D_{s0}^*(2317)$ in channel $DK(I=0)$ is reasonable. Global fitting can be performed after the coupling constant involving $D_{s0}^*(2317)$ is determined. We can see that $D_{s0}^*(2317)$ affects only the S -wave behavior of the

$DK(I = 0)$ channel in this method. The P -wave behavior should not be affected by $D_{s0}^*(2317)$ because $D_{s0}^*(2317)$ is always interpreted as a DK molecule with $I(J^P) = 0(0^+)$. However, the P -wave behavior can be improved by including the vector heavy mesons. We will discuss the issue in a forthcoming calculation.

5.2 Phase shifts

In the following, we make predictions of the S - and P -wave phase shifts for the eleven channels at the physical meson values using the LECs from Table 1. We use the values of the physical parameters: $m_\pi = 139.57$ MeV, $m_K = 493.68$ MeV, $f_\pi = 92.07$ MeV, $f_K = 110.03$ MeV, $M_D = 1869.66$ MeV, $M_{D_s} = 1968.35$ MeV from PDG [90]. The numerical results of the phase shifts of the pion-, kaon-, antikaon-, and eta-D meson scatterings are shown in Figs. 3, 4, 5, and 6, respectively. The error bands of the phase shifts in the total contributions are estimated from the statistical errors of the LECs using the standard error propagation formula with the correlations. We can see that the bands from the LECs are not too large to be unacceptable. The bands in the different orders are not given because we do not determine the LECs at the corresponding orders, although we present the values of the phase shifts from the different orders. The convergence is not good for most of the S -wave phase shifts, which is not surprising because it is difficult to achieve good convergence at the third chiral order, as in the case of the pion-nucleon scattering in Ref. [9]. However, the P -wave phase shifts at the third chiral order are much smaller than those at the second chiral order, which indicates good convergence. In Figs. 3, 4, 5, and 6, we also show the S -wave phase shifts calculated by the unitary method from Refs. [91,92] for making a more detailed comparison.

For the pion- D meson phase shifts, we obtain the repulsions in the $D\pi(I = 3/2)$ S wave and all P waves, and attractions in the $D\pi(I = 1/2)$ and $D_s\pi$ S waves. It is clear that there exist no bound states or resonances in the channels with repulsions. The attraction is weak below 200 MeV in the $D_s\pi$ S wave. The attraction should not be strong enough to generate a bound state or resonance in this wave. The $D\pi(I = 1/2)$ S wave is particularly interesting. The attraction exists at each order, and the total attraction is very strong even below 200 MeV. The results from lattice QCD simulations at nonphysical meson values support that there exists a bound state or resonance in this channel [83,93]. However, the production of a bound state or resonance requires nonperturbative dynamics through an iterated method. We can see that the same direction is obtained between our calculations and the unitary results for the S -wave phase shifts. More detailed calculations including nonperturbative dynamics will be presented in forthcoming work.

For the kaon- D meson phase shifts, there are repulsions in the D_sK S wave and all P waves, and thus the bound state or resonance cannot be dynamically generated in these waves. The $DK(I = 1)$ S wave has weak attractions that cannot generate a bound state or resonance. As expected, we obtain a strong attraction in the $DK(I = 0)$ S wave, while the result from the unitary method has the opposite sign. This wave corresponds to the well-known bound state $D_{s0}^*(2317)$. However, this exotic state has not been directly obtained in our perturbative calculation. Nevertheless, it is not difficult to obtain $D_{s0}^*(2317)$ by using an iterated method (e.g., Schrödinger equation) with the strong attractive DK interaction potential. The iterated method can generate the bound state because the nonperturbative dynamics are considered, as done in Refs. [91,92]. A more detailed description of $D_{s0}^*(2317)$ will also be given in forthcoming work.

For the antikaon- D meson phase shifts, the $D\bar{K}(I = 1)$ S wave and all P waves have repulsions. Apparently, the bound state or resonance cannot be found in these waves. Surprisingly, we obtain strong attractions in both $D\bar{K}(I = 0)$ and $D_s\bar{K}$ S waves. The first-order contribution almost cancels the second-order contribution in the $D\bar{K}(I = 0)$ S wave, and the third-order contribution dominates this wave. However, the total contribution is still very large. The resulting strong attraction in this wave is consistent with the lattice QCD result, which indicates that there exists a virtual bound state in the $D\bar{K}(I = 0)$ S wave [68]. In the $D_s\bar{K}$ S wave, the attraction is obtained from each order. The total attraction is very strong and supports the existence of a bound state. This wave corresponds to the possible $D_0^*(2400)$ signal based on the coupled-channel analysis of the $D\pi$, $D\eta$ and $D_s\bar{K}$ scattering amplitudes in Ref. [94]. This is also consistent with the strong attraction in the $D\pi(I = 1/2)$ S wave. There are also different signs between our perturbative calculation and the unitary result in this wave.

For the eta- D meson phase shifts, there are repulsions in all P waves and strong attractions in all S waves. The first- and third-order contributions are almost zero in both $D\eta$ and $D_s\eta$ S waves since the tree amplitudes at the first- and third-order are zero, and the one-loop amplitudes at the third order are small. The $D\eta$ S wave also corresponds to the $D_0^*(2400)$ in the coupled-channel $D\pi$, $D\eta$ and $D_s\bar{K}$ scattering amplitudes [94]. It is interesting that the $D_s\eta$ S wave also has strong attractions and supports the existence of a bound state or resonance, while the opposite signs exist from the unity results of the Refs. [91,92]. This will be further studied in future work.

From the phase shifts for the light pseudoscalar meson and heavy meson scattering, we can see that there are repulsions in all P waves, and the bound states or resonances cannot be dynamically generated in these waves. However, we find that the phase shifts in the $D\pi(I = 1/2)$, $DK(I = 0)$, $D\bar{K}(I = 0)$, $D_s\bar{K}$, $D\eta$ and $D_s\eta$ S waves are so strong that

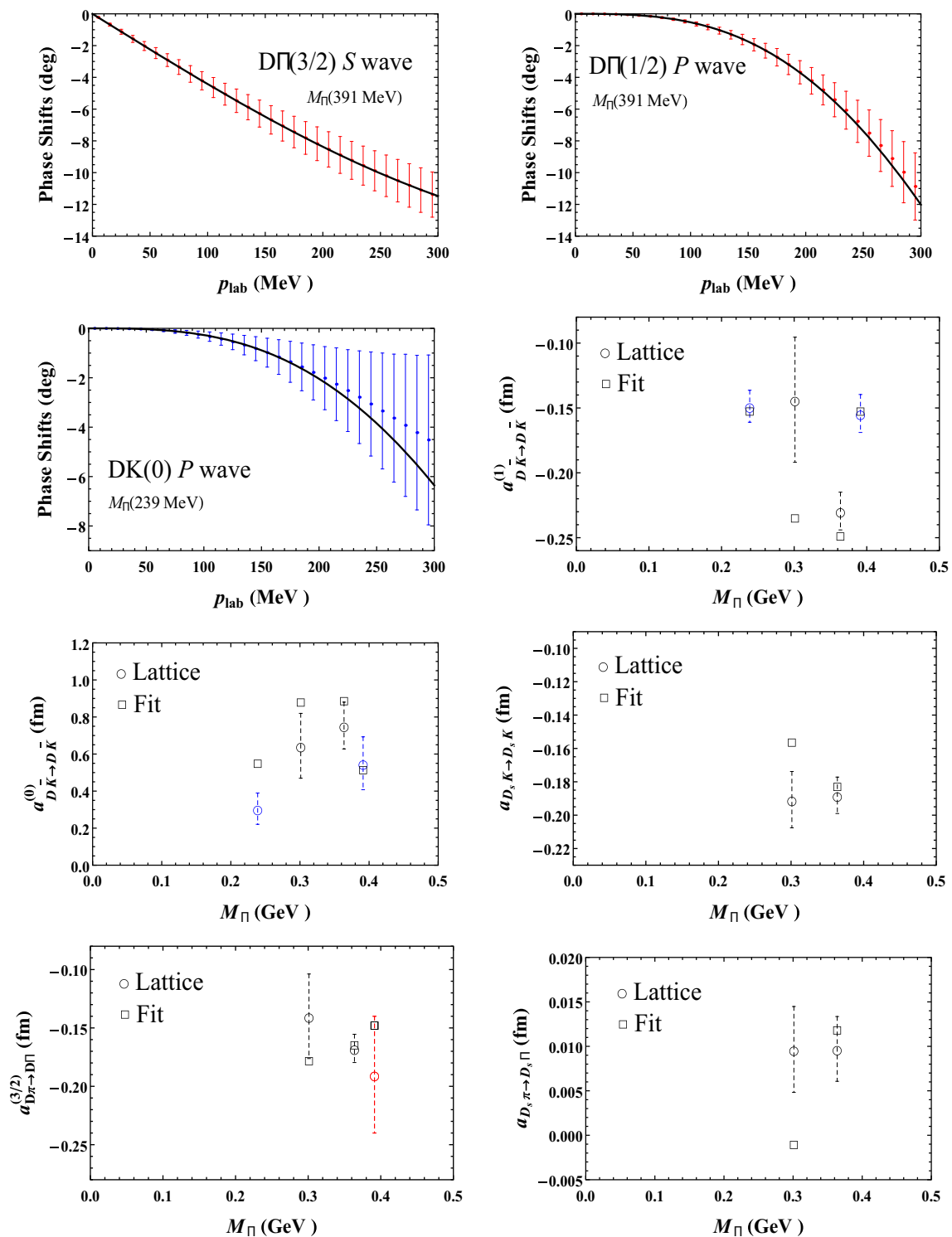


Fig. 2 Fits for the light pseudoscalar meson and D meson phase shifts and scattering lengths from various lattice data. The lattice phase shifts and scattering length with the red error bars in the $D\pi(I = 3/2)$ S -wave, $D\pi(I = 1/2)$ P -wave and $a_{D\bar{K} \to D\bar{K}}^{(3/2)}$ are from Ref. [83]. The lat-

tice data with the blue error bars in the $DK(I = 0)$ P -wave, $a_{D\bar{K} \to D\bar{K}}^{(1)}$ and $a_{D\bar{K} \to D\bar{K}}^{(0)}$ are from Ref. [68]. The lattice scattering lengths with the black error bars are from Ref. [65]. For a detailed description of the fits, see the main text

Table 2 Results of fitting by using the linear combinations of the low-energy constants. For a detailed description, see the main text

	Values	$c_0 + c_1$	$c_2 + c_4$	$c_3 + c_5$	\bar{k}_1	\bar{k}_2	\bar{k}_3
$c_0 + c_1$ (GeV^{-1})	0.04 ± 0.02	1.00	0.01	-0.47	-0.22	-0.79	0.00
$c_2 + c_4$ (GeV^{-1})	0.89 ± 0.02		1.00	-0.09	0.01	0.01	0.00
$c_3 + c_5$ (GeV^{-1})	-0.32 ± 0.04			1.00	0.95	0.77	0.00
\bar{k}_1 (GeV^{-2})	0.21 ± 0.07				1.00	0.60	0.00
\bar{k}_2 (GeV^{-2})	-7.13 ± 0.34					1.00	-0.39
\bar{k}_3 (GeV^{-2})	6.11 ± 0.14						1.00
$\chi^2/\text{d.o.f.}$	$\frac{147}{195-6} = 0.78$						

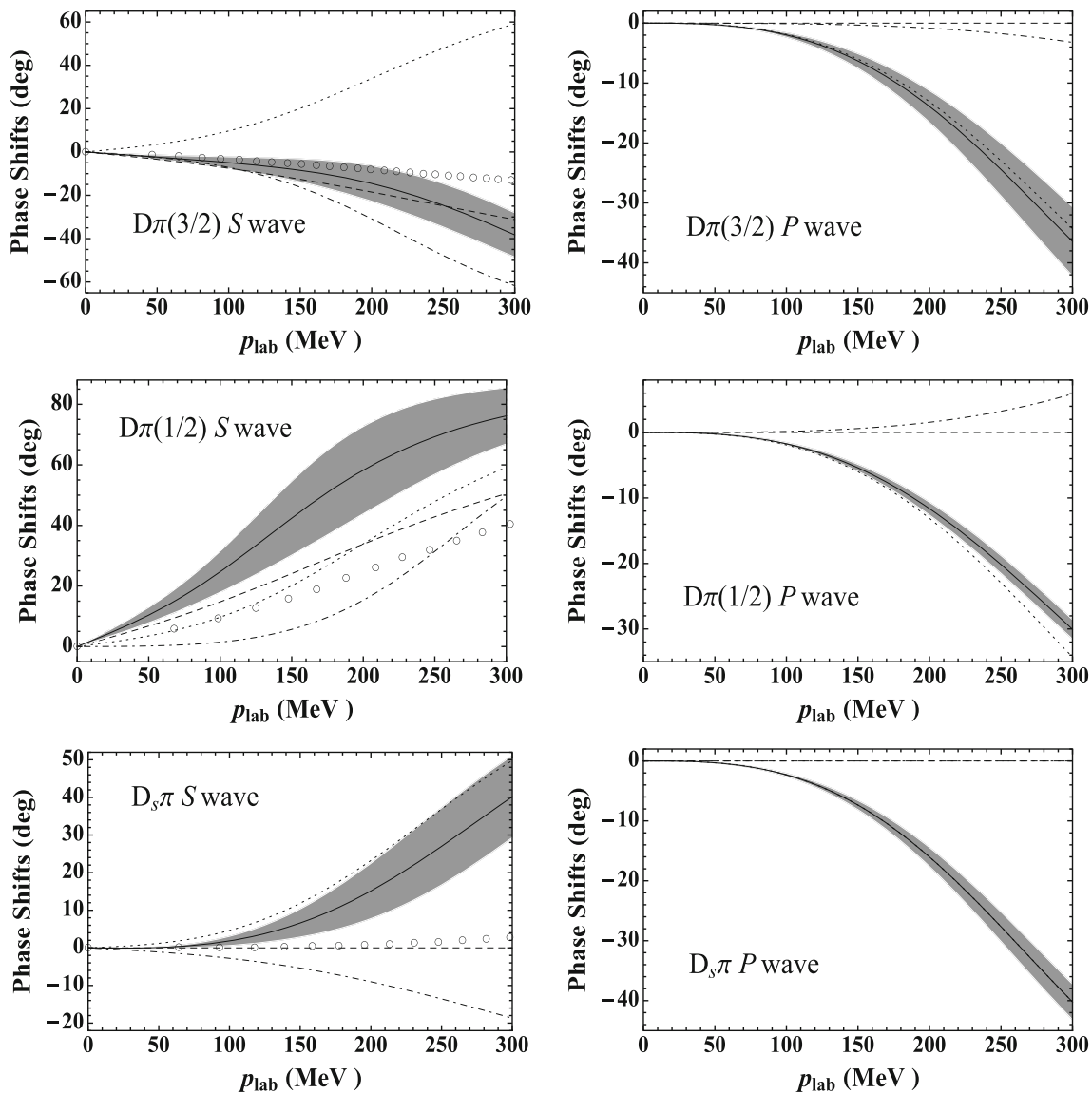


Fig. 3 Predictions for the pion- D meson phase shifts versus the pion laboratory momentum at physical meson values. The dashed, dotted, dash-dotted and solid lines denote the first-, second-, third-order, and their total contributions, respectively. The open circles present the uni-

tary results from Refs. [91,92]. The error bands are estimated from the statistical errors of the LECs using the standard error propagation formula with the correlations

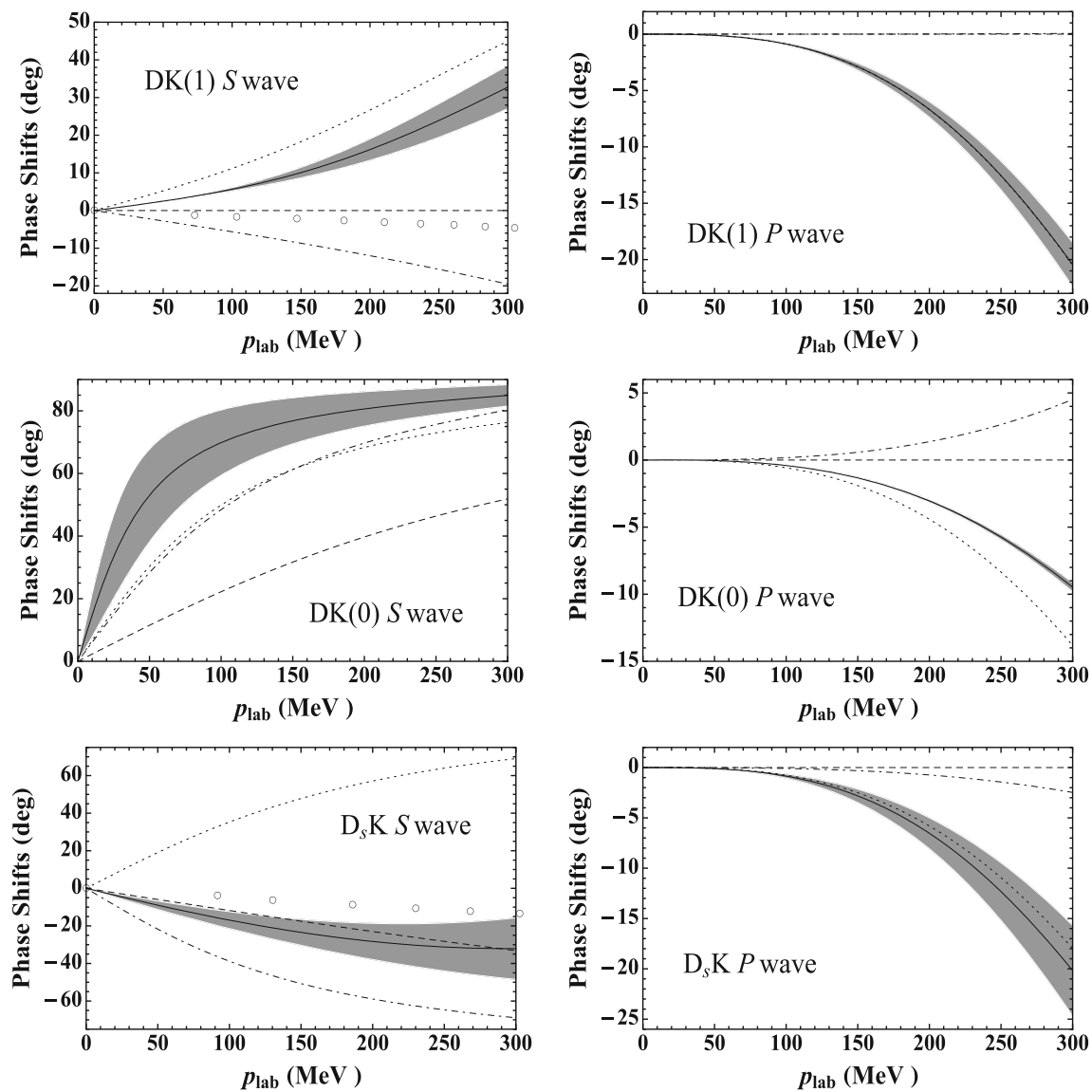


Fig. 4 Predictions for the kaon- D meson phase shifts versus the kaon laboratory momentum at physical meson values. The notation is the same as in Fig. 3

the bound states or resonances may be generated dynamically in these channels.

5.3 Scattering lengths and scattering volumes

Finally, we calculate the scattering lengths for the S waves and the scattering volumes for the P waves with Eq. (47) at the physical meson values. Analytical expressions for the threshold parameters can be found in Appendix 8. The scattering lengths are shown in Table 3, and the scattering volumes are shown in Table 4. The errors of the scattering lengths and the scattering volumes in our calculations are estimated from the statistical errors of the LECs using the error propagation formula with the correlations. Similarly,

the errors at the different orders are not given, although we present the values of the scattering lengths and the scattering volumes from the different orders. Good convergence is not achieved for the scattering lengths, while good convergence is obtained for the scattering volumes.

The scattering lengths in the channels $D\pi(I = 1/2)$, $DK(I = 0)$, $D\bar{K}(I = 0)$, $D_s\bar{K}$, $D\eta$ and $D_s\eta$ have large values. A bound state or resonance may be generated in these channels. The other scattering lengths are either small or negative, where a bound state or resonance cannot be dynamically generated. We obtain a large positive value for the channel $DK(I = 0)$, which corresponds to $D_{s0}^*(2317)$. A channel with a bound state should have a large negative scattering length, as obtained from Refs. [65, 79]. The correct scatter-

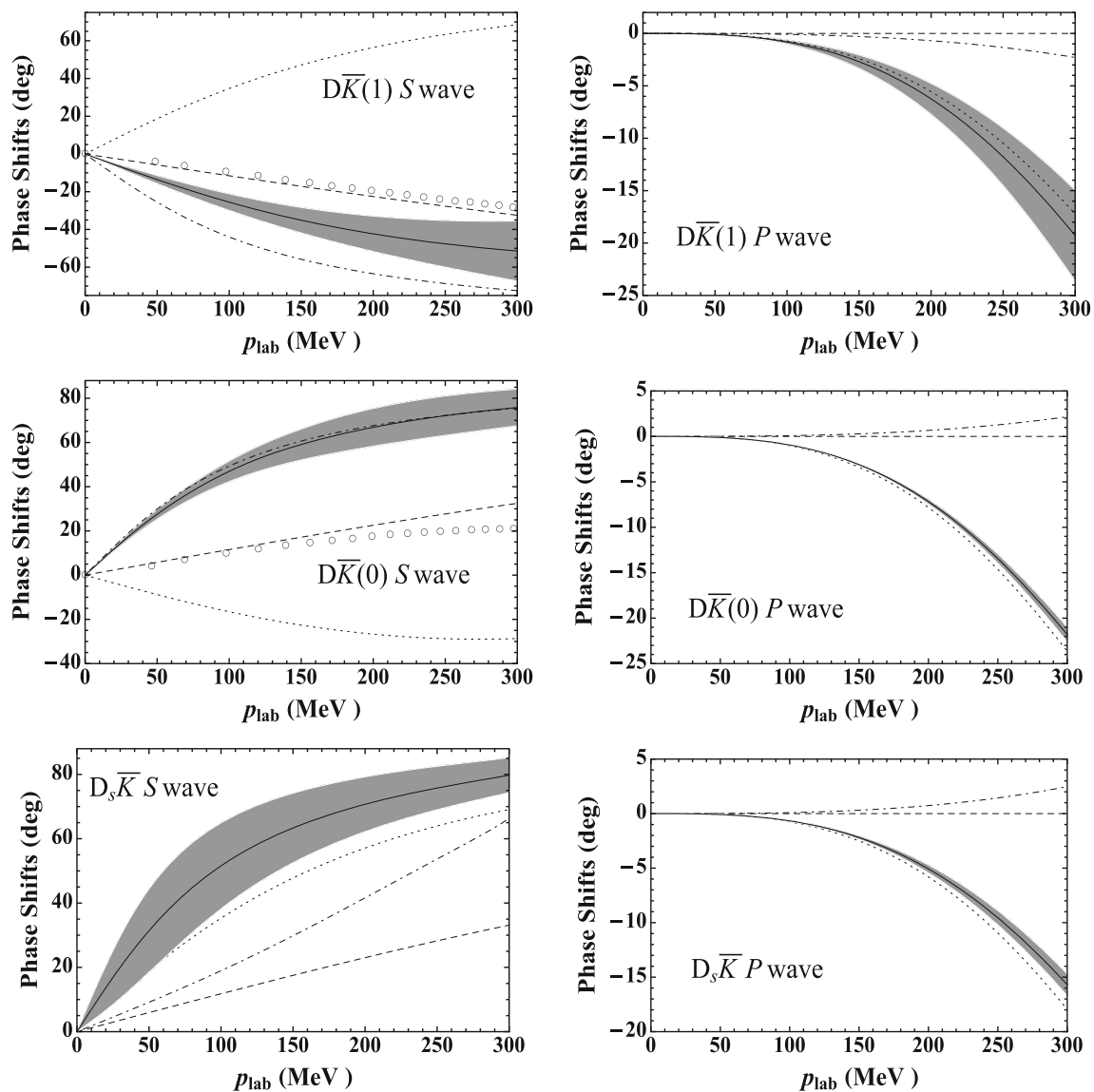


Fig. 5 Predictions for the antikaon- D meson phase shifts versus the antikaon laboratory momentum at physical meson values. The notation is the same as in Fig. 3

ing length for this channel was obtained in our previous work [72] through the iterated method.

We obtain the negative values for the scattering volumes in all channels. Therefore, a bound state or resonance cannot be generated in the P waves. The values from the first-order contributions are zero, and the values from the third-order contributions are small. Then, the second-order contributions dominate the total values. Good convergence is obtained for the scattering volumes at the third chiral order.

6 Summary

In summary, we have calculated the complete T matrices of the elastic light pseudoscalar meson and heavy meson scat-

tering up to the third order in HMChPT. We fitted the phase shifts and the scattering lengths from lattice QCD at non-physical meson values to determine the LECs. This led to a good description of the phase shifts below the 200 MeV pion/kaon momentum and the scattering lengths at the non-physical meson values for the channels excluding a bound state or resonance. We also obtained the LEC uncertainties and their mutual correlations through statistical regression analysis. We predicted the S - and P -wave phase shifts for light pseudoscalar meson and heavy meson scattering using these LECs at the physical meson values. We found that the phase shifts in the $D\pi(I = 1/2)$, $DK(I = 0)$, $D\bar{K}(I = 0)$, $D_s\bar{K}$, $D\eta$ and $D_s\eta$ S waves are strong enough to generate a bound state or resonance. The channel $DK(I = 0)$ corresponds to the well-known $D_{s0}^*(2317)$. The coupled channels

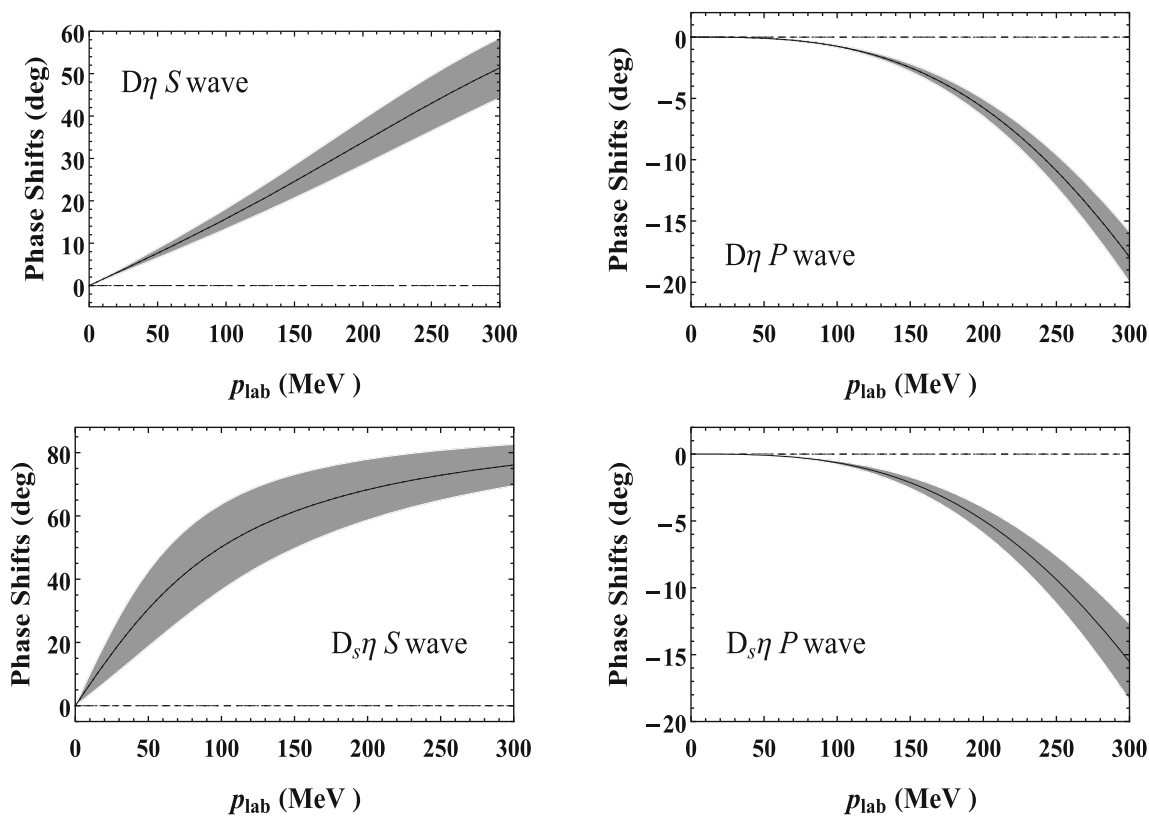


Fig. 6 Predictions for the eta-D meson phase shifts versus the eta laboratory momentum. The notation is the same as in Fig. 3

$D\pi(I = 1/2)$, $D_s\bar{K}$ and $D\eta$ may correspond to $D_0^*(2400)$. The channels $D\bar{K}(I = 0)$ and $D_s\eta$ may generate the respective bound state or resonance. However, as expected, we cannot obtain directly a bound state or resonance in our perturbative calculations. This issue can be successfully solved by the nonperturbative method, and the calculations including the nonperturbative dynamics will be presented in a forthcoming work. The P wave phase shifts in all channels are repulsive, and the bound states or resonances cannot be dynamically generated in these waves. We also predicted the scattering lengths and the scattering volumes using the LECs at the physical meson values. The scattering lengths also have large values in the channels $D\pi(I = 1/2)$, $DK(I = 0)$, $D\bar{K}(I = 0)$, $D_s\bar{K}$, $D\eta$ and $D_s\eta$, which indicate that a bound state or resonance may be generated in these channels. However, the correct scattering lengths for these channels should be obtained through the iterated method. We obtained negative values for the scattering volumes in all channels, and a bound state or resonance cannot be generated in the P waves. In addition, we obtained good convergence for the scattering volumes at the third chiral order. In order to study the bound states or resonances directly, the calculation including the nonperturbative dynamics is necessary. We hope our present calculations contribute to the investigations on the heavy meson–heavy meson interactions in HMChPT.

7 $D_{s0}^*(2317)$ contribution

Denoting the $D_{s0}^*(2317)$ by D_R , the leading-order effective Lagrangian with D_R as explicit degree of freedom reads

$$\mathcal{L}_{D_R} = \bar{D}_R(i v \cdot \partial - M_R + M_D)D_R + (g_R \langle \bar{D}_R v \cdot A D \rangle + \text{h.c.}) \tag{A.1}$$

where $A = \frac{\partial_\mu K}{f}$ with $K = (K^+, K^0)^T$ or $(K^-, \bar{K}^0)^T$, and $D = (D^0, D^+)$. The leading $D_{s0}^*(2317)$ -exchange Born-term contribution resulting from Fig. 7 reads

$$T_{KD}^{(0)} = \frac{2w_K^2 g_R^2}{f_K^2} \left(\frac{1}{M_R - M_D - w_K} + \frac{1}{M_R - M_D + w_K} \right). \tag{A.2}$$

Putting the LO, NLO, N2LO amplitudes and the Eq. (A.2) together in $KD(I = 0)$ channel, we can obtain the complete s -wave scattering lengths

$$a_{KD}^{(0)} = \frac{M_D}{8\pi(M_D + m_K)f_K^2} \times \left[2m_K + 2(4c_0 + 4c_1 + c_2 + c_3 + c_4 + c_5) \right]$$

Table 3 Predictions of the scattering lengths for the light pseudoscalar meson and D meson at the physical meson values. The scattering lengths are in units of fm

Sca. Len.	$\mathcal{O}(p)$	$\mathcal{O}(p^2)$	$\mathcal{O}(p^3)$	Total	Liu2013 [65]	Guo2019 [79]
$a_{(0,D\pi)}^{(3/2)}$	-0.24	0.23	-0.16	-0.17(6)	-0.100(2)	$-0.103^{+0.003}_{-0.003}$
$a_{(0,D\pi)}^{(1/2)}$	0.48	0.23	0.00	0.71(16)	$0.37^{+0.03}_{-0.02}$	$0.40^{+0.03}_{-0.02}$
$a_{(0,D_s\pi)}$	0.00	0.06	-0.08	-0.02(0)	-0.002(1)	$0.012^{+0.003}_{-0.003}$
$a_{(0,DK)}^{(1)}$	0.00	0.45	-0.24	0.21(1)	$0.07^{+0.03}_{-0.03} + i0.17^{+0.02}_{-0.01}$	$-0.01^{+0.05}_{-0.03} + i0.39^{+0.04}_{-0.04}$
$a_{(0,DK)}^{(0)}$	1.01	2.90	2.65	6.57(318)	$-0.84^{+0.17}_{-0.22}$	$-1.51^{+0.72}_{-2.35}$
$a_{(0,D_sK)}$	-0.51	1.69	-1.96	-0.78(19)	-0.18(1)	$-0.20^{+0.01}_{-0.01}$
$a_{(0,D\bar{K})}^{(1)}$	-0.51	1.67	-2.38	-1.21(19)	-0.20(1)	$-0.20^{+0.01}_{-0.01}$
$a_{(0,D\bar{K})}^{(0)}$	0.51	-0.78	2.86	2.58(19)	0.84(15)	21.9
$a_{(0,D_s\bar{K})}$	0.51	1.69	0.78	2.98(161)	$-0.09^{+0.06}_{-0.05} + i0.44^{+0.05}_{-0.05}$	$-0.57^{+0.06}_{-0.04} + i0.35^{+0.08}_{-0.07}$
$a_{(0,D\eta)}$	0.00	0.67	0.00	0.67(9)		$0.29^{+0.15}_{-0.22} + i0.61^{+0.30}_{-0.26}$
$a_{(0,D_s\eta)}$	0.00	2.97	0.00	2.97(139)		$-0.39^{+0.05}_{-0.03} + i0.06^{+0.02}_{-0.02}$

Table 4 Predictions of the scattering volumes for the light pseudoscalar meson and D meson at the physical meson values. The scattering volumes are in units of fm^3 . Note that, the values for the $\mathcal{O}(p)$ in all channels are zero, and are not shown

Sca. Vol.	$\mathcal{O}(p^2)$	$\mathcal{O}(p^3)$	Total
$a_{(1,D\pi)}^{(3/2)}$	-0.33	-0.01	-0.34(6)
$a_{(1,D\pi)}^{(1/2)}$	-0.33	0.02	-0.31(4)
$a_{(1,D_s\pi)}$	-0.40	0.00	-0.40(4)
$a_{(1,DK)}^{(1)}$	-0.24	0.00	-0.24(2)
$a_{(1,DK)}^{(0)}$	-0.16	0.05	-0.11(0)
$a_{(1,D_sK)}$	-0.20	-0.02	-0.22(5)
$a_{(1,D\bar{K})}^{(1)}$	-0.20	-0.02	-0.22(5)
$a_{(1,D\bar{K})}^{(0)}$	-0.28	0.02	-0.26(1)
$a_{(1,D_s\bar{K})}$	-0.20	0.02	-0.18(1)
$a_{(1,D\eta)}$	-0.22	0.00	-0.22(3)
$a_{(1,D_s\eta)}$	-0.18	0.00	-0.18(3)

$$\begin{aligned}
 & \times m_K^2 + 4(4\bar{\kappa}_1 + \bar{\kappa}_2 + \bar{\kappa}_3)m_K^3 \\
 & + \frac{3m_K^2}{8\pi^2 f_K^2} \left(m_K - \sqrt{m_\eta^2 - m_K^2} \arccos \frac{-m_K}{m_\eta} \right) \\
 & + 2m_K^2 g_R^2 \left(\frac{1}{M_R - M_D - m_K} + \frac{1}{M_R - M_D + m_K} \right) \Big]. \tag{A.3}
 \end{aligned}$$

8 Threshold parameters

In this appendix, we give the analytical expressions for the threshold parameters up to third order. These read:

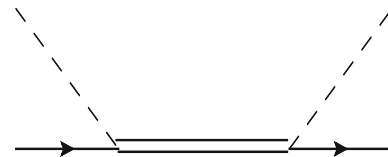


Fig. 7 The leading $D_{s0}^*(2317)$ -exchange Born-term contribution. The double solid, solid and dashed lines represent $D_{s0}^*(2317)$, D meson, and kaon, respectively. The crossed diagram is not shown

$$\begin{aligned}
 a_{(0,\pi D)}^{(1/2)} &= \frac{M_D}{8\pi(M_D + m_\pi)f_\pi^2} \\
 & \times \left[2m_\pi + (8c_0 + 4c_1 + 2c_2 + c_3 + 2c_4 + c_5) \right. \\
 & \times m_\pi^2 + 4(4\bar{\kappa}_1 + \bar{\kappa}_2 + \bar{\kappa}_3)m_\pi^3 \\
 & \left. - \frac{m_\pi^2}{16\pi^2 f_\pi^2} \left(6m_\pi + \sqrt{m_K^2 - m_\pi^2} \arccos \frac{m_\pi}{m_K} \right. \right. \\
 & \left. \left. - 3\sqrt{m_K^2 - m_\pi^2} \arccos \frac{-m_\pi}{m_K} \right) \right], \tag{B.1}
 \end{aligned}$$

$$\begin{aligned}
 a_{(1,\pi D)}^{(1/2)} &= \frac{M_D}{16\pi(M_D + m_\pi)f_\pi^2} \\
 & \times \left(-\frac{4}{3}c_4 - \frac{2}{3}c_5 - \frac{8}{3}\bar{\kappa}_3 m_\pi + \frac{7}{864\pi^2 f_\pi^2} m_\pi \right), \tag{B.2}
 \end{aligned}$$

$$\begin{aligned}
 a_{(0,\pi D)}^{(3/2)} &= \frac{M_D}{8\pi(M_D + m_\pi)f_\pi^2} \\
 & \times \left[-m_\pi + (8c_0 + 4c_1 + 2c_2 + c_3 + 2c_4 + c_5) \right. \\
 & \times m_\pi^2 - 2(4\bar{\kappa}_1 + \bar{\kappa}_2 + \bar{\kappa}_3)m_\pi^3 \\
 & \left. - \frac{m_\pi^2}{16\pi^2 f_\pi^2} \left(3m_\pi + 2\sqrt{m_K^2 - m_\pi^2} \arccos \frac{m_\pi}{m_K} \right) \right], \tag{B.3}
 \end{aligned}$$

$$a_{(1,\pi D)}^{(3/2)} = \frac{M_D}{16\pi(M_D + m_\pi)f_\pi^2} \left(-\frac{4}{3}c_4 - \frac{2}{3}c_5 + \frac{4}{3}\bar{\kappa}_3 m_\pi \right)$$

$$-\frac{7}{432\pi^2 f_\pi^2} m_\pi), \quad (\text{B.4})$$

$$a_{(0,\pi D_s)} = \frac{M_{D_s}}{8\pi(M_{D_s} + m_\pi) f_\pi^2} \left[2(4c_0 + c_2 + c_4) m_\pi^2 - \frac{m_\pi^2}{8\pi f_\pi^2} \sqrt{m_K^2 - m_\pi^2} \right], \quad (\text{B.5})$$

$$a_{(1,\pi D_s)} = \frac{M_{D_s}}{16\pi(M_{D_s} + m_\pi) f_\pi^2} \left(-\frac{4}{3} c_4 \right), \quad (\text{B.6})$$

$$a_{(0,KD)}^{(1)} = \frac{M_D}{8\pi(M_D + m_K) f_K^2} \left\{ 2(4c_0 + c_2 + c_4) m_K^2 + \frac{m_K^2}{8\pi^2 f_K^2} \times \left[\sqrt{m_K^2 - m_\pi^2} \left(i\pi - \ln \frac{m_K + \sqrt{m_K^2 - m_\pi^2}}{m_\pi} \right) \right] \right\}, \quad (\text{B.7})$$

$$a_{(1,KD)}^{(1)} = \frac{M_D}{16\pi(M_D + m_K) f_K^2} \left(-\frac{4}{3} c_4 + \frac{m_K}{288\pi^2 f_K^2} \right), \quad (\text{B.8})$$

$$a_{(0,KD)}^{(0)} = \frac{M_D}{8\pi(M_D + m_K) f_K^2} \times \left[2m_K + 2(4c_0 + 4c_1 + c_2 + c_3 + c_4 + c_5) \times m_K^2 + 4(4\bar{k}_1 + \bar{k}_2 + \bar{k}_3) m_K^3 + \frac{3m_K^2}{8\pi^2 f_K^2} \left(m_K - \sqrt{m_\eta^2 - m_K^2} \arccos \frac{-m_K}{m_\eta} \right) \right], \quad (\text{B.9})$$

$$a_{(1,KD)}^{(0)} = \frac{M_D}{16\pi(M_D + m_K) f_K^2} \left(-\frac{4}{3} c_4 - \frac{4}{3} c_5 - \frac{8\bar{k}_3}{3} m_K - \frac{23}{864\pi^2 f_K^2} m_K \right), \quad (\text{B.10})$$

$$a_{(0,KD_s)} = \frac{M_{D_s}}{8\pi(M_{D_s} + m_K) f_K^2} \times \left[-m_K + (8c_0 + 4c_1 + 2c_2 + c_3 + 2c_4 + c_5) \times m_K^2 - (8\bar{k}_1 + 2\bar{k}_2 + 2\bar{k}_3) m_K^3 - \frac{3m_K^2}{16\pi^2 f_K^2} \left(m_K + \sqrt{m_\eta^2 - m_K^2} \arccos \frac{m_K}{m_\eta} - \sqrt{m_K^2 - m_\pi^2} \ln \frac{m_K + \sqrt{m_K^2 - m_\pi^2}}{m_\pi} \right) \right], \quad (\text{B.11})$$

$$a_{(1,KD_s)} = \frac{M_{D_s}}{16\pi(M_{D_s} + m_K) f_K^2} \times \left(-\frac{4}{3} c_4 - \frac{2}{3} c_5 + \frac{4\bar{k}_3}{3} m_K + \frac{7}{864\pi^2 f_K^2} m_K \right), \quad (\text{B.12})$$

$$a_{(0,\bar{K}D)}^{(1)} = \frac{M_D}{8\pi(M_D + m_K) f_K^2} \times \left[-m_K + (8c_0 + 4c_1 + 2c_2 + c_3 + 2c_4 + c_5) \times m_K^2 - (8\bar{k}_1 + 2\bar{k}_2 + 2\bar{k}_3) m_K^3 + \frac{m_K^2}{16\pi^2 f_K^2} \left(-3m_K - 3\sqrt{m_\eta^2 - m_K^2} \arccos \frac{m_K}{m_\eta} + \sqrt{m_K^2 - m_\pi^2} \ln \frac{m_K + \sqrt{m_K^2 - m_\pi^2}}{m_\pi} \right) \right], \quad (\text{B.13})$$

$$a_{(1,\bar{K}D)}^{(1)} = \frac{M_D}{16\pi(M_D + m_K) f_K^2} \times \left(-\frac{4}{3} c_4 - \frac{2}{3} c_5 + \frac{4\bar{k}_3}{3} m_K + \frac{5}{432\pi^2 f_K^2} m_K \right), \quad (\text{B.14})$$

$$a_{(0,\bar{K}D)}^{(0)} = \frac{M_D}{8\pi(M_D + m_K) f_K^2} \times \left[m_K + (8c_0 - 4c_1 + 2c_2 - c_3 + 2c_4 - c_5) \times m_K^2 + (8\bar{k}_1 + 2\bar{k}_2 + 2\bar{k}_3) m_K^3 + \frac{3m_K^2}{16\pi^2 f_K^2} \left(m_K + \sqrt{m_\eta^2 - m_K^2} \arccos \frac{m_K}{m_\eta} + \sqrt{m_K^2 - m_\pi^2} \ln \frac{m_K + \sqrt{m_K^2 - m_\pi^2}}{m_\pi} \right) \right], \quad (\text{B.15})$$

$$a_{(1,\bar{K}D)}^{(0)} = \frac{M_D}{16\pi(M_D + m_K) f_K^2} \times \left(-\frac{4}{3} c_4 + \frac{2}{3} c_5 - \frac{4\bar{k}_3}{3} m_K - \frac{1}{54\pi^2 f_K^2} m_K \right), \quad (\text{B.16})$$

$$a_{(0,\bar{K}D_s)} = \frac{M_{D_s}}{8\pi(M_{D_s} + m_K) f_K^2} \times \left\{ m_K + (8c_0 + 4c_1 + 2c_2 + c_3 + 2c_4 + c_5) \times m_K^2 + (8\bar{k}_1 + 2\bar{k}_2 + 2\bar{k}_3) m_K^3 - \frac{3m_K^2}{16\pi^2 f_K^2} \times \left[m_K - \sqrt{m_\eta^2 - m_K^2} \arccos \frac{-m_K}{m_\eta} + \left(i\pi - \sqrt{m_K^2 - m_\pi^2} \ln \frac{m_K + \sqrt{m_K^2 - m_\pi^2}}{m_\pi} \right) \right] \right\}, \quad (\text{B.17})$$

$$a_{(1,\bar{K}D_s)} = \frac{M_{D_s}}{16\pi(M_{D_s} + m_K) f_K^2} \times \left(-\frac{4}{3} c_4 - \frac{2}{3} c_5 - \frac{4\bar{k}_3}{3} m_K - \frac{7}{864\pi^2 f_K^2} m_K \right), \quad (\text{B.18})$$

$$a_{(0,\eta D)} = \frac{M_D}{8\pi(M_D + m_\eta) f_\eta^2} \left\{ \frac{1}{9} [4(24c_0 + 6c_2 + c_3 + 6c_4 + c_5) \times m_K^2 - (24c_0 - 12c_1 + 6c_2 + c_3 + 6c_4 + c_5) \times m_\pi^2] + \frac{3m_\eta^2}{16\pi^2 f_\eta^2} (i\pi) \right\}, \quad (\text{B.19})$$

$$a_{(1,\eta D)} = \frac{M_D}{16\pi(M_D + m_\eta) f_\eta^2} \left(-\frac{4}{3} c_4 - \frac{2}{9} c_5 \right), \quad (\text{B.20})$$

$$a_{(0,\eta D_s)} = \frac{M_{D_s}}{8\pi(M_{D_s} + m_\eta) f_\eta^2} \left\{ \frac{1}{9} [8(12c_0 + 12c_1 + 3c_2 + 2c_3 + 3c_4 + 2c_5) m_K^2 - 2(12c_0 + 24c_1 + 3c_2 + 2c_3 + 3c_4 + 2c_5) m_\pi^2] + \frac{3m_\eta^2}{8\pi^2 f_\eta^2} (i\pi) \right\}, \quad (\text{B.21})$$

$$a_{(1,\eta D_s)} = \frac{M_{D_s}}{16\pi(M_{D_s} + m_\eta) f_\eta^2} \left(-\frac{4}{3} c_4 - \frac{8}{9} c_5 \right). \quad (\text{B.22})$$

Acknowledgements This work is supported by the National Natural Science Foundation of China under Grants No. 11975033, No. 12070131001 and No. 12147127, and China Postdoctoral Science Foundation (Grant No. 2021M700251). We thank Xiao-Yu Guo (Beijing University of Technology), Feng-Kun Guo (Beijing, Institute of Theoretical Physics), Jing Ou-Yang (Yunnan University) and Norbert Kaiser (Technische Universität München) for very helpful discussions.

Data Availability Statement This manuscript has no associated data or the data will not be deposited. [Authors' comment: It is a theory paper and there are no data attached to it.]

Open Access This article is licensed under a Creative Commons Attribution 4.0 International License, which permits use, sharing, adaptation, distribution and reproduction in any medium or format, as long as you give appropriate credit to the original author(s) and the source, provide a link to the Creative Commons licence, and indicate if changes were made. The images or other third party material in this article are included in the article's Creative Commons licence, unless indicated otherwise in a credit line to the material. If material is not included in the article's Creative Commons licence and your intended use is not permitted by statutory regulation or exceeds the permitted use, you will need to obtain permission directly from the copyright holder. To view a copy of this licence, visit <http://creativecommons.org/licenses/by/4.0/>.

Funded by SCOAP³. SCOAP³ supports the goals of the International Year of Basic Sciences for Sustainable Development.

References

1. S. Weinberg, Phenomenological Lagrangians. *Physica A* **96**, 327–340 (1979). [https://doi.org/10.1016/0378-4371\(79\)90223-1](https://doi.org/10.1016/0378-4371(79)90223-1)
2. S. Scherer, M.R. Schindler, A primer for chiral perturbation theory. *Lect. Notes Phys.* **830**, 1–338 (2012). <https://doi.org/10.1007/978-3-642-19254-8>
3. R. Machleidt, D.R. Entem, Chiral effective field theory and nuclear forces. *Phys. Rep.* **503**, 1–75 (2011). <https://doi.org/10.1016/j.physrep.2011.02.001>
4. J. Gasser, M.E. Sainio, A. Svarc, Nucleons with chiral loops. *Nucl. Phys. B* **307**, 779–853 (1988). [https://doi.org/10.1016/0550-3213\(88\)90108-3](https://doi.org/10.1016/0550-3213(88)90108-3)
5. E.E. Jenkins, A.V. Manohar, Baryon chiral perturbation theory using a heavy fermion Lagrangian. *Phys. Lett. B* **255**, 558–562 (1991). [https://doi.org/10.1016/0370-2693\(91\)90266-S](https://doi.org/10.1016/0370-2693(91)90266-S)
6. V. Bernard, N. Kaiser, J. Kambor, U.-G. Meißner, Chiral structure of the nucleon. *Nucl. Phys. B* **388**, 315–345 (1992). [https://doi.org/10.1016/0550-3213\(92\)90615-1](https://doi.org/10.1016/0550-3213(92)90615-1)
7. C. Ordóñez, U. van Kolck, Chiral lagrangians and nuclear forces. *Phys. Lett. B* **291**, 459–464 (1992). [https://doi.org/10.1016/0370-2693\(92\)91404-W](https://doi.org/10.1016/0370-2693(92)91404-W)
8. E. Epelbaum, W. Glöckle, U.-G. Meißner, Nuclear forces from chiral lagrangians using the method of unitary transformation (I): formalism. *Nucl. Phys. A* **637**, 107–134 (1998). [https://doi.org/10.1016/S0375-9474\(98\)00220-6](https://doi.org/10.1016/S0375-9474(98)00220-6)
9. N. Fettes, U.-G. Meißner, S. Steininger, Pion-nucleon scattering in chiral perturbation theory (I): isospin symmetric case. *Nucl. Phys. A* **640**, 199–234 (1998). [https://doi.org/10.1016/S0375-9474\(98\)00452-7](https://doi.org/10.1016/S0375-9474(98)00452-7)
10. N. Fettes, U.-G. Meißner, Pion nucleon scattering in chiral perturbation theory (II): fourth order calculation. *Nucl. Phys. A* **676**, 311 (2000). [https://doi.org/10.1016/S0375-9474\(00\)00199-8](https://doi.org/10.1016/S0375-9474(00)00199-8)
11. Norbert Kaiser, R. Brockmann, W. Weise, Peripheral nucleon–nucleon phase shifts and chiral symmetry. *Nucl. Phys. A* **625**, 758–788 (1997). [https://doi.org/10.1016/S0375-9474\(97\)00586-1](https://doi.org/10.1016/S0375-9474(97)00586-1)
12. X.-W. Kang, J. Haidenbauer, U.-G. Meißner, Antinucleon–nucleon interaction in chiral effective field theory. *JHEP* **02**, 113 (2014). [https://doi.org/10.1007/JHEP02\(2014\)113](https://doi.org/10.1007/JHEP02(2014)113)
13. D.R. Entem, N. Kaiser, R. Machleidt, Y. Nasyk, Peripheral nucleon–nucleon scattering at fifth order of chiral perturbation theory. *Phys. Rev. C* **91**, 014002 (2015). <https://doi.org/10.1103/PhysRevC.91.014002>
14. N. Kaiser, Density-dependent NN interaction from subsubleading chiral 3N forces: intermediate-range contributions. *Phys. Rev. C* **101**, 014001 (2020). <https://doi.org/10.1103/PhysRevC.101.014001>
15. N. Kaiser, Chiral corrections to kaon nucleon scattering lengths. *Phys. Rev. C* **64**, 045204 (2001). <https://doi.org/10.1103/PhysRevC.64.045204>
16. Y.-R. Liu, S.-L. Zhu, Meson-baryon scattering lengths in HB χ PT. *Phys. Rev. D* **75**, 034003 (2007). <https://doi.org/10.1103/PhysRevD.75.034003>
17. J. Haidenbauer, S. Petschauer, N. Kaiser, U.-G. Meißner, A. Nogga, W. Weise, Hyperon–nucleon interaction at next-to-leading order in chiral effective field theory. *Nucl. Phys. A* **915**, 24–58 (2013). <https://doi.org/10.1016/j.nuclphysa.2013.06.008>
18. B.-L. Huang, Y.-D. Li, Kaon–nucleon scattering to one-loop order in heavy baryon chiral perturbation theory. *Phys. Rev. D* **92**, 114033 (2015). <https://doi.org/10.1103/PhysRevD.92.114033>
19. B.-L. Huang, J.-S. Zhang, Y.-D. Li, N. Kaiser, Meson–baryon scattering to one-loop order in heavy baryon chiral perturbation theory. *Phys. Rev. D* **96**, 016021 (2017). <https://doi.org/10.1103/PhysRevD.96.016021>
20. B.-L. Huang, J. Ou-Yang, Pion–nucleon scattering to $\mathcal{O}(p^3)$ in heavy baryon SU(3) chiral perturbation theory. *Phys. Rev. D* **101**, 056021 (2020). <https://doi.org/10.1103/PhysRevD.101.056021>
21. B.-L. Huang, Pion–nucleon scattering to order p^4 in SU(3) heavy baryon chiral perturbation theory. *Phys. Rev. D* **102**, 116001 (2020). <https://doi.org/10.1103/PhysRevD.102.116001>
22. B.-L. Huang, J.-B. Cheng, S.-L. Zhu, Peripheral nucleon–nucleon scattering at next-to-next-to-leading order in SU(3) heavy baryon chiral perturbation theory. *Phys. Rev. D* **104**, 116030 (2021). <https://doi.org/10.1103/PhysRevD.104.116030>
23. T. Becher, H. Leutwyler, Baryon chiral perturbation theory in manifestly Lorentz invariant form. *Eur. Phys. J. C* **9**, 643–671 (1999). <https://doi.org/10.1007/PL00021673>
24. J. Gegelia, G. Japaridze, Matching heavy particle approach to relativistic theory. *Phys. Rev. D* **60**, 114038 (1999). <https://doi.org/10.1103/PhysRevD.60.114038>
25. T. Fuchs, J. Gegelia, G. Japaridze, S. Scherer, Renormalization of relativistic baryon chiral perturbation theory and power counting. *Phys. Rev. D* **68**, 056005 (2003). <https://doi.org/10.1103/PhysRevD.68.056005>
26. M.R. Schindler, T. Fuchs, J. Gegelia, S. Scherer, Axial, induced pseudoscalar, and pion-nucleon form-factors in manifestly Lorentz-invariant chiral perturbation theory. *Phys. Rev. C* **75**, 025202 (2007). <https://doi.org/10.1103/PhysRevC.75.025202>
27. L.S. Geng, J. Martin Camalich, L. Alvarez-Ruso, M.J. Vicente Vacas, Leading SU(3)-breaking corrections to the baryon magnetic moments in chiral perturbation theory. *Phys. Rev. Lett.* **101**, 222002 (2008). <https://doi.org/10.1103/PhysRevLett.101.222002>
28. J.M. Alarcón, J. Martín Camalich, J.A. Oller, The chiral representation of the πN scattering amplitude and the pion–nucleon sigma term. *Phys. Rev. D* **85**, 051503 (2012). <https://doi.org/10.1103/PhysRevD.85.051503>
29. X.L. Ren, L.S. Geng, J. Martin Camalich, J. Meng, H. Toki, Octet baryon masses in next-to-next-to-next-to-leading order covariant baryon chiral perturbation theory. *JHEP* **12**, 073 (2012). [https://doi.org/10.1007/JHEP12\(2012\)073](https://doi.org/10.1007/JHEP12(2012)073)
30. Y.-H. Chen, D.-L. Yao, H.Q. Zheng, Analyses of pion–nucleon elastic scattering amplitudes up to $\mathcal{O}(p^4)$ in extended-on-mass-

- shell subtraction scheme. Phys. Rev. D **87**, 054019 (2013). <https://doi.org/10.1103/PhysRevD.87.054019>
31. D.-L. Yao, D. Siemens, V. Bernard, E. Epelbaum, A.M. Gasparyan, J. Gegelia, H. Krebs, U.-G. Meißner, Pion-nucleon scattering in covariant baryon chiral perturbation theory with explicit Delta resonances. JHEP **05**, 038 (2016). [https://doi.org/10.1007/JHEP05\(2016\)038](https://doi.org/10.1007/JHEP05(2016)038)
 32. J.-X. Lu, C.-X. Wang, Y. Xiao, L.-S. Geng, J. Meng, P. Ring, Accurate relativistic chiral nucleon–nucleon interaction up to next-to-next-to-leading order. Phys. Rev. Lett. **128**, 142002 (2022). <https://doi.org/10.1103/PhysRevLett.128.142002>
 33. M.B. Wise, Chiral perturbation theory for hadrons containing a heavy quark. Phys. Rev. D **45**, R2188 (1992). <https://doi.org/10.1103/PhysRevD.45.R2188>
 34. B. Wang, L. Meng, S.-L. Zhu, Hidden-charm and hidden-bottom molecular pentaquarks in chiral effective field theory. JHEP **11**, 108 (2019). [https://doi.org/10.1007/JHEP11\(2019\)108](https://doi.org/10.1007/JHEP11(2019)108)
 35. L. Meng, B. Wang, S.-L. Zhu, $\Sigma_c N$ interaction in chiral effective field theory. Phys. Rev. C **101**, 064002 (2020). <https://doi.org/10.1103/PhysRevC.101.064002>
 36. B. Wang, L. Meng, S.-L. Zhu, $D^{(*)}N$ interaction and the structure of $\Sigma_c(2800)$ and $\Lambda_c(2940)$ in chiral effective field theory. Phys. Rev. D **101**, 094035 (2020). <https://doi.org/10.1103/PhysRevD.101.094035>
 37. K. Chen, B.-L. Huang, B. Wang, S.-L. Zhu, $\Sigma_c \Sigma_c$ interactions in chiral effective field theory (2022). [arXiv:2204.13316](https://arxiv.org/abs/2204.13316)
 38. L. Meng, B. Wang, G.-J. Wang, S.-L. Zhu, Chiral perturbation theory for heavy hadrons and chiral effective field theory for heavy hadronic molecules (2022). [arXiv:2204.08716](https://arxiv.org/abs/2204.08716)
 39. B. Aubert et al., Observation of a narrow meson decaying to $D_s^+ \pi^0$ at a mass of 2.32-GeV/ c^2 . Phys. Rev. Lett. **90**, 242001 (2003). <https://doi.org/10.1103/PhysRevLett.90.242001>
 40. P. Krokovny et al., Observation of the $D_{sJ}(2317)$ and $D_{sJ}(2457)$ in B decays. Phys. Rev. Lett. **91**, 262002 (2003). <https://doi.org/10.1103/PhysRevLett.91.262002>
 41. D. Besson et al., Observation of a narrow resonance of mass 2.46 GeV/ c^2 decaying to $D_s^{*+} \pi^0$ and confirmation of the $D_{sJ}^+(2317)$ state. Phys. Rev. D **68**, 032002 (2003). <https://doi.org/10.1103/PhysRevD.68.032002>
 42. S.K. Choi et al., Observation of a narrow charmonium-like state in exclusive $B^\pm \rightarrow K^\pm \pi^+ \pi^- J/\psi$ decays. Phys. Rev. Lett. **91**, 262001 (2003). <https://doi.org/10.1103/PhysRevLett.91.262001>
 43. X. Liu, An overview of XYZ new particles. Chin. Sci. Bull. **59**, 3815–3830 (2014). <https://doi.org/10.1007/s11434-014-0407-2>
 44. J.-J. Xie, W.-H. Liang, E. Oset, Hidden charm pentaquark and $\Lambda(1405)$ in the $\Lambda_b^0 \rightarrow \eta_c K^- p(\pi\Sigma)$ reaction. Phys. Lett. B **777**, 447–452 (2018). <https://doi.org/10.1016/j.physletb.2017.12.064>
 45. Y.-L. Ma, M. Harada, Chiral partner structure of doubly heavy baryons with heavy quark spin-flavor symmetry. J. Phys. G **45**, 075006 (2018). <https://doi.org/10.1088/1361-6471/aac86e>
 46. Y.-R. Liu, H.-X. Chen, W. Chen, X. Liu, S.-L. Zhu, Pentaquark and tetraquark states. Prog. Part. Nucl. Phys. **107**, 237–320 (2019). <https://doi.org/10.1016/j.pnpnp.2019.04.003>
 47. W.-H. Liang, N. Ikeno, E. Oset, $\Upsilon(nI)$ decay into $B^{(*)} \bar{B}^{(*)}$. Phys. Lett. B **803**, 135340 (2020). <https://doi.org/10.1016/j.physletb.2020.135340>
 48. Y. Dong, P. Shen, F. Huang, Z. Zhang, Selected strong decays of pentaquark state $P_c(4312)$ in a chiral constituent quark model. Eur. Phys. J. C **80**, 341 (2020). <https://doi.org/10.1140/epjc/s10052-020-7890-1>
 49. Wu, Qi, Dian-Yong. Chen, Wen-Hua. Qin, Gang Li, Production of Z_{cs} in B and B_s decays. Eur. Phys. J. C **82**(6), 520 (2022). <https://doi.org/10.1140/epjc/s10052-022-10465-z>
 50. C. Deng, S.-L. Zhu, T_{cc}^+ and its partners. Phys. Rev. D **105**, 054015 (2022). <https://doi.org/10.1103/PhysRevD.105.054015>
 51. Cheng-Rong. Deng, Shi-Lin. Zhu, Decoding the double heavy tetraquark state T_{cc}^+ . Sci. Bull. **67**, 1522 (2022). <https://doi.org/10.1016/j.scib.2022.06.016>
 52. J. He, X. Liu, The quasi-fission phenomenon of double charm T_{cc}^+ induced by nucleon. Eur. Phys. J. C **82**, 387 (2022). <https://doi.org/10.1140/epjc/s10052-022-10363-4>
 53. Hua-Xing. Chen, Wei Chen, Xiang Liu, Yan-Rui. Liu, Shi-Lin. Zhu, An updated review of the new hadron states. Rep. Prog. Phys. **86**(2), 026201 (2023). <https://doi.org/10.1088/1361-6633/aca3b6>
 54. Zhi-Hui. Wang, Guo-Li. Wang, Two-body strong decays of the 2P and 3P charmonium states. Phys. Rev. D **106**(5), 054037 (2022). <https://doi.org/10.1103/PhysRevD.106.054037>
 55. L.R. Dai, R. Molina, E. Oset, Looking for the exotic X0(2866) and its JP=1+ partner in the $B^-0 \rightarrow D^{(*)}+K-K^{(*)}0$ reactions. Phys. Rev. D **105**(9), 096022 (2022). <https://doi.org/10.1103/PhysRevD.105.096022>
 56. T. Barnes, F.E. Close, H.J. Lipkin, Implications of a DK molecule at 2.32 GeV. Phys. Rev. D **68**, 054006 (2003). <https://doi.org/10.1103/PhysRevD.68.054006>
 57. E. van Beveren, G. Rupp, Observed $D_s(2317)$ and tentative $d(2100-2300)$ as the charmed cousins of the light scalar nonet. Phys. Rev. Lett. **91**, 012003 (2003). <https://doi.org/10.1103/PhysRevLett.91.012003>
 58. G.S. Bali, $D_{sJ}^+(2317)$: what can the lattice say? Phys. Rev. D **68**, 071501 (2003). <https://doi.org/10.1103/PhysRevD.68.071501>
 59. V. Dmitrašinović, $D_{s0}^+(2317)-D_0(2308)$ mass difference as evidence for tetraquarks. Phys. Rev. Lett. **94**, 162002 (2005). <https://doi.org/10.1103/PhysRevLett.94.162002>
 60. F.-K. Guo, P.-N. Shen, H.-C. Chiang, R.-G. Ping, B.-S. Zou, Dynamically generated 0^+ heavy mesons in a heavy chiral unitary approach. Phys. Lett. B **641**, 278–285 (2006). <https://doi.org/10.1016/j.physletb.2006.08.064>
 61. F.-K. Guo, P.-N. Shen, H.-C. Chiang, Dynamically generated 1^+ heavy mesons. Phys. Lett. B **647**, 133–139 (2007). <https://doi.org/10.1016/j.physletb.2007.01.050>
 62. J.M. Flynn, J. Nieves, Elastic s-wave $B\pi$, $D\pi$, DK and $K\pi$ scattering from lattice calculations of scalar form-factors in semileptonic decays. Phys. Rev. D **75**, 074024 (2007). <https://doi.org/10.1103/PhysRevD.75.074024>
 63. M.F.M. Lutz, M. Soyeur, Radiative and isospin-violating decays of D(s)-mesons in the hadrogenesis conjecture. Nucl. Phys. A **813**, 14–95 (2008). <https://doi.org/10.1016/j.nuclphysa.2008.09.003>
 64. D. Mohler, C.B. Lang, L. Leskovec, S. Prelovsek, R.M. Woloshyn, $D_{s0}^*(2317)$ meson and D-meson-kaon scattering from lattice QCD. Phys. Rev. Lett. **111**, 222001 (2013). <https://doi.org/10.1103/PhysRevLett.111.222001>
 65. L. Liu, K. Orginos, F.-K. Guo, C. Hanhart, U.-G. Meißner, Interactions of charmed mesons with light pseudoscalar mesons from lattice QCD and implications on the nature of the $D_{s0}^*(2317)$. Phys. Rev. D **87**, 014508 (2013). <https://doi.org/10.1103/PhysRevD.87.014508>
 66. C. Alexandrou, J. Berlin, J. Finkenrath, T. Leontiou, M. Wagner, Tetraquark interpolating fields in a lattice QCD investigation of the $D_{s0}^*(2317)$ meson. Phys. Rev. D **101**, 034502 (2020). <https://doi.org/10.1103/PhysRevD.101.034502>
 67. Y. Tan, J. Ping, $D_{s0}^*(2317)$ and $D_{s1}(2460)$ in an unquenched quark model (2021). [arXiv:2111.04677](https://arxiv.org/abs/2111.04677)
 68. G.K.C. Cheung, C.E. Thomas, D.J. Wilson, G. Moir, M. Peardon, S. Ryan, DK I = 0, $D\bar{K}$ I = 0, 1 scattering and the $D_{s0}^*(2317)$ from lattice QCD. JHEP **02**, 100 (2021). [https://doi.org/10.1007/JHEP02\(2021\)100](https://doi.org/10.1007/JHEP02(2021)100)
 69. Z. Yang, G.-J. Wang, J.-J. Wu, M. Oka, S.-L. Zhu, Novel coupled channel framework connecting the quark model and lattice QCD for the near-threshold Ds states. Phys. Rev. Lett. **128**, 112001 (2022). <https://doi.org/10.1103/PhysRevLett.128.112001>

70. H.-X. Chen, W. Chen, X. Liu, Y.-R. Liu, S.-L. Zhu, A review of the open charm and open bottom systems. *Rep. Prog. Phys.* **80**, 076201 (2017). <https://doi.org/10.1088/1361-6633/aa6420>
71. Y.-R. Liu, X. Liu, S.-L. Zhu, Light pseudoscalar meson and heavy meson scattering lengths. *Phys. Rev. D* **79**, 094026 (2009). <https://doi.org/10.1103/PhysRevD.79.094026>
72. B.-L. Huang, Z.-Y. Lin, S.-L. Zhu, Light pseudoscalar meson and heavy meson scattering lengths to $\mathcal{O}(p^4)$ in heavy meson chiral perturbation theory. *Phys. Rev. D* **105**, 036016 (2022). <https://doi.org/10.1103/PhysRevD.105.036016>
73. E.E. Kolomeitsev, M.F.M. Lutz, On heavy light meson resonances and chiral symmetry. *Phys. Lett. B* **582**, 39–48 (2004). <https://doi.org/10.1016/j.physletb.2003.10.118>
74. F.-K. Guo, C. Hanhart, U.-G. Meißner, Interactions between heavy mesons and Goldstone bosons from chiral dynamics. *Eur. Phys. J. A* **40**, 171–179 (2009). <https://doi.org/10.1140/epja/i2009-10762-1>
75. L.S. Geng, N. Kaiser, J. Martin-Camalich, W. Weise, Low-energy interactions of nambu-goldstone bosons with d mesons in covariant chiral perturbation theory. *Phys. Rev. D* **82**, 054022 (2010). <https://doi.org/10.1103/PhysRevD.82.054022>
76. P. Wang, X.G. Wang, Publisher's note: Study of 0^+ states with open charm in the unitarized heavy meson chiral approach [*Phys. Rev. D* 86, 014030 (2012)]. *Phys. Rev. D* **86**, 039903 (2012). <https://doi.org/10.1103/PhysRevD.86.039903>
77. M. Altenbuchinger, L.-S. Geng, W. Weise, Scattering lengths of Nambu–Goldstone bosons off D mesons and dynamically generated heavy-light mesons. *Phys. Rev. D* **89**, 014026 (2014). <https://doi.org/10.1103/PhysRevD.89.014026>
78. D.-L. Yao, M.-L. Du, F.-K. Guo, U.-G. Meißner, One-loop analysis of the interactions between charmed mesons and Goldstone bosons. *JHEP* **11**, 058 (2015). [https://doi.org/10.1007/JHEP11\(2015\)058](https://doi.org/10.1007/JHEP11(2015)058)
79. Z.-H. Guo, L. Liu, U.-G. Meißner, J.A. Oller, A. Rusetsky, Towards a precise determination of the scattering amplitudes of the charmed and light-flavor pseudoscalar mesons. *Eur. Phys. J. C* **79**, 13 (2019). <https://doi.org/10.1140/epjc/s10052-018-6518-1>
80. B. Borasoy, U.-G. Meißner, Chiral expansion of baryon masses and sigma-terms. *Ann. Phys.* **254**, 192–232 (1997). <https://doi.org/10.1006/aphy.1996.5630>
81. J. Gasser, U.-G. Meißner, On the phase of epsilon-prime. *Phys. Lett. B* **258**, 219–224 (1991). [https://doi.org/10.1016/0370-2693\(91\)91235-N](https://doi.org/10.1016/0370-2693(91)91235-N)
82. T.E.O. Ericson, W. Weise, *Pions and Nuclei* (Clarendon Press, Oxford, 1988)
83. G. Moir, M. Peardon, S. Ryan, C.E. Thomas, D.J. Wilson, Coupled-channel $D\pi$, $D\eta$ and $D_s\bar{K}$ scattering from lattice QCD. *JHEP* **10**, 011 (2016). [https://doi.org/10.1007/JHEP10\(2016\)011](https://doi.org/10.1007/JHEP10(2016)011)
84. A. Walker-Loud et al., Light hadron spectroscopy using domain wall valence quarks on an asqtad sea. *Phys. Rev. D* **79**, 054502 (2009). <https://doi.org/10.1103/PhysRevD.79.054502>
85. J. Dobaczewski, W. Nazarewicz, P.-G. Reinhard, Error estimates of theoretical models: a guide. *J. Phys. G* **41**, 074001 (2014). <https://doi.org/10.1088/0954-3899/41/7/074001>
86. B.D. Carlsson et al., Uncertainty analysis and order-by-order optimization of chiral nuclear interactions. *Phys. Rev. X* **6**, 011019 (2016). <https://doi.org/10.1103/PhysRevX.6.011019>
87. C.C. Chang et al., A per-cent-level determination of the nucleon axial coupling from quantum chromodynamics. *Nature* **558**, 91–94 (2018). <https://doi.org/10.1038/s41586-018-0161-8>
88. B. Märkisch et al., Measurement of the weak axial-vector coupling constant in the decay of free neutrons using a pulsed cold neutron beam. *Phys. Rev. Lett.* **122**, 242501 (2019). <https://doi.org/10.1103/PhysRevLett.122.242501>
89. Chang-Hwan. Lee, Hong-Pil. Min, Mannque Rho, Kaon–nucleon scattering from chiral Lagrangians. *Phys. Lett. B* **326**, 14–20 (1994). [https://doi.org/10.1016/0370-2693\(94\)91185-1](https://doi.org/10.1016/0370-2693(94)91185-1)
90. P.A. Zyla et al., Review of particle physics. *Prog. Theor. Exp. Phys.* **2020**, 083C01 (2020). <https://doi.org/10.1093/ptep/ptaa104>
91. Xiao-Yu. Guo, Yonggoo Heo, Matthias F. M. Lutz, On chiral extrapolations of charmed meson masses and coupled-channel reaction dynamics. *Phys. Rev. D* **98**, 014510 (2018). <https://doi.org/10.1103/PhysRevD.98.014510>
92. Xiao-Yu. Guo, Yonggoo Heo, Matthias F. M. Lutz, From lattice QCD to predictions of scattering phase shifts at the physical point. *PoS LATTICE2021*, 601 (2022). <https://doi.org/10.22323/1.396.0601>
93. E.B. Gregory, F.-K. Guo, C. Hanhart, S. Krieg, T. Luu, Confirmation of the existence of an exotic state in the πD system (2021). [arXiv:2106.15391](https://arxiv.org/abs/2106.15391)
94. M. Albaladejo, P. Fernandez-Soler, F.-K. Guo, J. Nieves, Two-pole structure of the $D_0^*(2400)$. *Phys. Lett. B* **767**, 465–469 (2017). <https://doi.org/10.1016/j.physletb.2017.02.036>